PDGFRα signaling regulates Srsf3 transcript binding to affect PI3K signaling and endosomal trafficking

Thomas E. Forman[1,2], Marcin P. Sajek[3,4,5], Eric D. Larson[6,7], Neelanjan Mukherjee[3,4], Katherine A. Fantauzzo[1,4,*]

[1]Department of Craniofacial Biology, School of Dental Medicine, University of Colorado Anschutz Medical Campus, Aurora, CO, USA

[2]Medical Scientist Training Program, University of Colorado Anschutz Medical Campus, Aurora, CO, USA

[3]Department of Biochemistry and Molecular Genetics, School of Medicine, University of Colorado Anschutz Medical Campus, Aurora, CO, USA

[4]RNA Bioscience Initiative, University of Colorado Anschutz Medical Campus, Aurora, CO, USA

[5]Institute of Human Genetics, Polish Academy of Sciences, Poznan, Poland

[6]Department of Otolaryngology – Head and Neck Surgery, University of Colorado Anschutz Medical Campus, Aurora, CO, USA

[7]Basic and Translational Sciences, Penn Dental Medicine, University of Pennsylvania, Philadelphia, PA, USA

*Corresponding author. Email: katherine.fantauzzo@cuanschutz.edu

Abstract

Signaling through the platelet-derived growth factor receptor alpha (PDGFRα) plays a critical role in craniofacial development, as mutations in *PDGFRA* are associated with cleft lip/palate in humans and *Pdgfra* mutant mouse models display varying degrees of facial clefting. Phosphatidylinositol 3-kinase (PI3K)/Akt is the primary effector of PDGFRα signaling during skeletal development in the mouse. We previously demonstrated that Akt phosphorylates the RNA-binding protein serine/arginine-rich splicing factor 3 (Srsf3) downstream of PI3K-mediated PDGFRα signaling in mouse embryonic palatal mesenchyme (MEPM) cells, leading to its nuclear translocation. We further showed that ablation of *Srsf3* in the murine neural crest lineage results in severe midline facial clefting, due to defects in proliferation and survival of cranial neural crest cells, and widespread alternative RNA splicing (AS) changes. Here, we sought to determine the molecular mechanisms by which Srsf3 activity is regulated downstream of PDGFRα signaling to control AS of transcripts necessary for craniofacial development. We demonstrated via enhanced UV-crosslinking and immunoprecipitation (eCLIP) of MEPM cells that PDGF-AA stimulation leads to preferential binding of Srsf3 to exons and loss of binding to canonical Srsf3 CA-rich motifs. Through the analysis of complementary RNA-seq data, we showed that Srsf3 activity results in the preferential inclusion of exons with increased GC content and lower intron to exon length ratio. Moreover, we found that the subset of transcripts that are bound by Srsf3 and undergo AS upon PDGFRα signaling commonly encode regulators of PI3K signaling and early endosomal trafficking. Functional validation studies further confirmed that Srsf3 activity downstream of PDGFRα signaling leads to retention of the receptor in early endosomes and increases in downstream PI3K-mediated Akt signaling. Taken together, our findings reveal that growth factor-mediated phosphorylation of an RNA-binding protein underlies gene expression regulation necessary for mammalian craniofacial development.

45 **Introduction**

46 Craniofacial development is a complex morphogenetic process that requires a precise
47 interplay of multiple cell and tissue types to generate the frontonasal skeleton. Disruption of this
48 process can result in some of the most common birth differences in humans, such as cleft lip
49 and palate (Mai et al., 2019). Signaling through the platelet derived growth factor receptor alpha
50 (PDGFRα) receptor tyrosine kinase (RTK) is essential for human craniofacial development.
51 Heterozygous missense mutations in the coding region of *PDGFRA* that alter amino acids within
52 the extracellular, transmembrane or cytoplasmic domains of the receptor, in addition to single
53 base-pair substitutions in the 3' untranslated region (3' UTR), are associated with nonsyndromic
54 cleft palate (Rattanasopha et al., 2012). Further, single-nucleotide polymorphisms that repress
55 transcriptional activity of the promoter upstream of *PDGFC*, which encodes one of two PDGFRα
56 ligands, are associated with cleft lip and palate (Choi et al., 2009). This role of PDGFRα
57 signaling in craniofacial development is conserved in mice, as *Pdgfra* mutant mouse models
58 display a variety of defects that range from cleft palate to complete facial clefting (Klinghoffer et
59 al., 2002; Soriano, 1997; Tallquist & Soriano, 2003; Fantauzzo & Soriano, 2014; He & Soriano,
60 2013). These phenotypes are recapitulated in embryos lacking both *Pdgfa* and *Pdgfc* (Ding et
61 al., 2004). Phosphatidylinositol 3-kinase (PI3K) is the primary effector of PDGFRα signaling
62 during skeletal development in the mouse (Klinghoffer et al., 2002). Following activation, PI3K
63 increases phosphatidylinositol-3,4,5-trisphosphate (PIP_3) levels at the cell membrane, leading to
64 the recruitment and subsequent phosphorylation of the serine/threonine kinase Akt. Akt
65 subsequently dissociates from the membrane to phosphorylate an array of target proteins that
66 are involved in wide-ranging cellular processes (Manning & Cantley, 2007). We previously
67 identified proteins phosphorylated by Akt downstream of PI3K-mediated PDGFRα signaling in
68 primary mouse embryonic mesenchyme (MEPM) cells (Fantauzzo & Soriano, 2014). Gene

69 ontology analysis revealed that 25% of the 56 proteins were involved in RNA processing, with a
70 particular enrichment for RNA splicing (Fantauzzo & Soriano, 2014).

71 Alternative RNA splicing (AS) is a process by which different combinations of exons from
72 the same gene are incorporated into mature RNA transcripts, thereby contributing to gene
73 expression regulation and enhancing the diversity of protein isoforms (Licatalosi & Darnell,
74 2010). AS occurs in approximately 95% of multi-exon human genes, frequently in a tissue-
75 specific manner (Pan et al., 2008; Wang et al., 2008). Dysregulation of AS causes a number of
76 diseases due to mutations in precursor RNA sequences, mutations in core components of the
77 spliceosome complex and/or mutations in auxiliary RNA-binding proteins (RBPs) (Scotti &
78 Swanson, 2016). These *trans*-acting auxiliary RBPs bind to specific sequence and/or structural
79 motifs in a target RNA via one or more RNA-binding domains to promote or inhibit exon
80 inclusion (Fu & Ares, 2014; Licatalosi & Darnell, 2010). The phenotypes resulting from global
81 and/or tissue-specific knockout of multiple RBPs have established that RBP-mediated AS is an
82 essential process during mouse craniofacial development (Bebee et al., 2015; Cibi et al., 2019;
83 Dennison et al., 2021; Forman et al., 2021; Lee et al., 2020). We previously demonstrated that
84 ablation of *Srsf3* in the murine neural crest lineage results in severe midline facial clefting and
85 facial bone hypoplasia, due to defects in proliferation and survival of cranial neural crest cells,
86 and widespread AS changes (Dennison et al., 2021).

87 Srsf3 belongs to the serine/arginine-rich (SR) protein family of splicing factors that
88 generally promote exon inclusion by binding to exonic and intronic splicing enhancers and by
89 recruiting spliceosome components to the 5' and 3' splice sites (Fu & Ares, 2014; Licatalosi &
90 Darnell, 2010). Srsf3 specifically was shown to bind pyrimidine-rich motifs, with a preference for
91 exonic regions (Akerman et al., 2009; Änkö et al., 2012). Srsf3 is phosphorylated downstream of
92 PDGF and EGF stimulation and all-*trans* retinoic acid treatment, and by the kinases Akt and
93 SRPK2 (Bavelloni et al., 2014; Dennison et al., 2021; Fantauzzo & Soriano, 2014; Long et al.,
94 2019; Zhou et al., 2012). Phosphorylation of the Akt consensus sites within the C-terminal

95 arginine/serine-rich (RS) domain of Srsf3 drives its translocation to the nucleus, where AS takes
96 place (Bavelloni et al., 2014; Dennison et al., 2021; Long et al., 2019). Moreover,
97 phosphorylation of the RS domain can alter the ability of SR proteins to interact with other
98 proteins, such as the U1 small nuclear ribonucleoprotein (snRNP) component of the
99 spliceosome and additional RBPs, and affect the ability of SR proteins to bind RNA (Huang et
100 al., 2004; Shen & Green, 2006; Shin et al., 2004; Xiao & Manley, 1997). However, the molecular
101 mechanisms by which Srsf3 activity is regulated downstream of specific signaling inputs in a
102 context-specific manner to regulate RNA binding and/or sequence specificity remain
103 undetermined.

104 Here, we identified changes in Srsf3-dependent AS and Srsf3 transcript binding in the
105 absence or presence of PDGF-AA ligand in MEPM cells. RNA-sequencing (RNA-seq) analysis
106 revealed that Srsf3 activity and PDGFRα signaling have more pronounced effects on AS than
107 gene expression, as well as a significant dependence in regulating AS. Using enhanced UV-
108 crosslinking and immunoprecipitation (eCLIP), we found a shift from intronic to exonic Srsf3
109 binding and loss of CA-rich sites upon PDGF-AA stimulation. Further, we demonstrated that the
110 subset of transcripts that are bound by Srsf3 and undergo AS upon PDGFRα signaling
111 commonly encode regulators of PI3K signaling and early endosomal trafficking, ultimately
112 serving as a feedback mechanism to affect trafficking of the receptors. Combined, our findings
113 provide significant insight into the mechanisms underlying RBP-mediated gene expression
114 regulation in response to growth factor stimulation within the embryonic mesenchyme.
115

116 **Results**

117 *PDGFRα signaling for one hour minimally affects gene expression*

118 To determine the Srsf3-dependent changes in gene expression and AS downstream of
119 PDGFRα signaling, we stably integrated a scramble shRNA (scramble) or an shRNA targeting

120 the 3' UTR of *Srsf3* (shSrsf3) into immortalized MEPM (iMEPM) cells via lentiviral transduction
121 (Fig. 1A). Western blotting revealed a 66% decrease in Srsf3 protein levels in the shSrsf3 cell
122 line (Fig. 1B). We previously demonstrated that phosphorylated Srsf3 levels peaked in the
123 nucleus of iMEPM cells following 1 hour of PDGF-AA ligand treatment (Dennison et al., 2021).
124 As such, cells were left unstimulated (-PDGF-AA) or treated with 10 ng/mL PDGF-AA for 1 hour
125 (+PDGF-AA). RNA was isolated and sequenced from three biological replicates across each of
126 the four conditions (Fig. 1A; Table S1). We first examined Srsf3-dependent differentially-
127 expressed (DE) genes by comparing scramble versus shSrsf3 samples across the same PDGF-
128 AA stimulation condition (-PDGF-AA or +PDGF-AA). We detected 827 DE genes in the absence
129 of ligand treatment and 802 DE genes upon ligand stimulation (Fig. 1C, Table S2). There was
130 extensive overlap (521 out of 1,108; 47.0%) of Srsf3-dependent DE genes across ligand
131 treatment conditions, resulting in a total of 1,108 unique genes within both datasets (Fig. 1C,D;
132 Fig. S1A). Of the 521 shared DE genes, 514 (98.7%) had the same directionality, including 273
133 (52%) with shared increases in expression in the shSrsf3 samples and 241 (46%) with shared
134 decreases in expression in the shSrsf3 samples (Fig. 1C,D). These findings demonstrate that
135 expression of a set of genes (521) depends on Srsf3 activity independent of PDGFRα signaling,
136 while a similarly sized set of genes (587) is differentially expressed in response to both Srsf3
137 activity and PDGFRα signaling (Fig. 1C,D). Gene ontology (GO) analysis of the Srsf3-
138 dependent DE genes revealed that the most significant terms for biological process commonly
139 involved regulation of osteoblast differentiation, calcium-dependent cell-cell adhesion, regulation
140 of cell migration and canonical Wnt signaling, while only a handful of significant terms for
141 molecular function were detected in unstimulated cells, relating to cation channel activity and
142 phosphatase activity (Fig. S2A,B).
143 We next examined PDGF-AA-dependent DE genes by comparing -PDGF-AA versus
144 +PDGF-AA across the same Srsf3 condition (scramble or shSrsf3). We detected only 37 DE

145 genes in scramble cells and 14 DE genes in shSrsf3 cells (Fig. 1E, Table S2). There was limited
146 overlap (4 out of 47; 8.51%) of PDGF-AA-dependent DE genes across Srsf3 conditions,
147 resulting in a total of 47 unique genes within both datasets (Fig. 1E,F; Fig. S1B). Of the 4
148 shared DE genes, 3 (75%) had shared increases in expression upon PDGF-AA stimulation (Fig.
149 1E,F). These findings demonstrate that, unlike Srsf3 activity, PDGFRα signaling minimally
150 affects gene expression at one hour of ligand stimulation, consistent with our previous findings
151 in mouse embryonic facial mesenchyme (Dennison et al., 2021). Further, these results show
152 that expression of a set of genes (4) depends on PDGFRα signaling independent of Srsf3
153 activity, while a larger set of genes (43) is differentially expressed in response to both PDGFRα
154 signaling and Srsf3 activity (Fig. 1E,F). GO analysis of the PDGF-AA-dependent DE genes
155 revealed significant terms for biological process in the scramble cells relating to cell migration,
156 response to growth factor stimulation and regulation of transcription (Fig. S2A). The most
157 significant terms for molecular function commonly involved DNA binding (Fig. S2B).
158
159 *PDGFRα signaling for one hour has a more pronounced effect on alternative RNA splicing*
160 We previously demonstrated that AS is an important mechanism of gene expression
161 regulation downstream of PI3K/Akt-mediated PDGFRα signaling in the murine mid-gestation
162 palatal shelves (Dennison et al., 2021). Accordingly, we next assessed AS in our same RNA-
163 seq dataset. In examining Srsf3-dependent alternatively-spliced transcripts, we detected 1,354
164 differential AS events in the absence of ligand treatment and 1,071 differential AS events upon
165 ligand stimulation (Fig. 2A). When filtered to include events detected in at least 10 reads in
166 either condition, we obtained a list of 1,113 differential AS events in the absence of ligand
167 treatment and 795 differential AS events upon ligand stimulation (Fig. 2B, Tables S3 and S4).
168 There was limited overlap (203 out of 1,705; 11.9%) of Srsf3-dependent alternatively-spliced
169 transcripts across ligand treatment conditions, resulting in a total of 1,705 unique events within

170 both datasets (Fig. 2A,B). Of the 203 shared alternatively-spliced transcripts, 100% had the
171 same directionality, including 81 (40%) with shared negative changes in percent spliced in (PSI)
172 (exon included more often in shSrsf3 samples) and 122 (60%) with shared positive changes in
173 PSI (exon skipped more often in shSrsf3 samples) (Fig. 2A,B). We confirmed the differential AS
174 of two transcripts, *Arhgap12* and *Cep55*, between scramble and shSrsf3 samples by qPCR
175 using primers within constitutively-expressed exons flanking the alternatively-spliced exon (Fig.
176 S3A,B). These findings demonstrate that AS of a set of transcripts (203) depends on Srsf3
177 activity independent of PDGFRα signaling, while a much larger set of transcripts (1,502) is
178 alternatively spliced in response to both Srsf3 activity and PDGFRα signaling (Fig. 2A,B). GO
179 analysis of these Srsf3-dependent alternatively-spliced transcripts revealed that the most
180 significant terms for biological process and molecular function commonly involved regulation of
181 RNA splicing, and RNA binding and cadherin binding, respectively (Fig. S4A,B).
182 In examining PDGF-AA-dependent alternatively-spliced transcripts, we detected 595
183 differential AS events in scramble cells and 398 differential AS events in shSrsf3 cells (Fig. 2C).
184 When filtered to include events detected in at least 10 reads in either condition, we obtained a
185 list of 375 differential AS events in scramble cells and 256 differential AS events in shSrsf3 cells
186 (Fig. 2D, Tables S5 and S6). There was negligible overlap (9 out of 622; 1.45%) of PDGF-AA-
187 dependent alternatively-spliced transcripts across Srsf3 conditions, resulting in a total of 622
188 unique events within both datasets (Fig. 2C,D). Of the 9 shared alternatively-spliced transcripts,
189 100% had the same directionality, including 5 (56%) with shared negative changes in PSI (exon
190 included more often in +PDGF-AA samples) and 4 (44%) with shared positive changes in PSI
191 (exon skipped more often in +PDGF-AA samples) (Fig. 2C,D). Taken together, these findings
192 demonstrate that both Srsf3 activity and PDGFRα signaling have more pronounced effects on
193 AS than gene expression. While more transcripts and genes are subject to these regulatory
194 mechanisms upon loss of Srsf3 activity, the magnitude of events is more greatly skewed

195 towards AS upon PDGF-AA stimulation. Further, these results show that AS of a set of
196 transcripts (9) depends on PDGFRα signaling independent of Srsf3 activity, while a much larger
197 set of transcripts (613) is alternatively spliced in response to both PDGFRα signaling and Srsf3
198 activity (Fig. 2C,D). When combined with the data above (Fig. 2B), this points to a profound
199 dependence between PDGFRα signaling and Srsf3 in regulating AS of transcripts in the facial
200 mesenchyme. GO analysis of these PDGF-AA-dependent alternatively-spliced transcripts
201 demonstrated only a handful of significant terms for molecular function in the scramble cells, all
202 relating to protein kinase activity (Fig. S4B).
203 The vast majority of Srsf3-dependent (70.2-73.7%) and PDGF-AA dependent (62.1-
204 65.1%) AS events involved skipped exons, with minimal contribution from retained introns,
205 mutually exclusive exons, alternative 5' splice sites, or alternative 3' splice sites (Fig. 2E). For
206 the Srsf3-dependent skipped exon events, there were more transcripts with +ΔPSI (exon
207 skipped more often in shSrsf3 samples) (44.8%) as opposed to -ΔPSI (exon included more
208 often in shSrsf3 samples) (25.4%) in the absence of PDGF-AA stimulation (Fig. 2E), consistent
209 with previous results that SR proteins tend to promote exon inclusion (Fu & Ares, 2014;
210 Licatalosi & Darnell, 2010). However, PDGF-AA ligand treatment led to an increase in the
211 percentage of transcripts with -ΔPSI (36.5%) (Fig. 2E), indicating that PDGFRα signaling
212 promotes exon skipping in the presence of Srsf3. Among the PDGF-AA-dependent skipped
213 exon events, there was a significant shift in transcripts with -ΔPSI (exon included more often in
214 +PDGF-AA samples) in the absence (41.0%) versus presence (19.5%) of Srsf3, and a
215 corresponding shift in transcripts with +ΔPSI (exon skipped more often in +PDGF-AA samples)
216 (21.1% and 45.6%, respectively) (Fig. 2E), again suggesting that PDGF-AA stimulation causes
217 increased exon skipping when Srsf3 is present.
218
219 *Srsf3 exhibits differential transcript binding upon PDGFRα signaling*

220 To determine direct binding targets of Srsf3 downstream of PDGFRα signaling, we
221 conducted eCLIP (Van Nostrand et al., 2016, 2017) of iMEPM cells that were left unstimulated (-
222 PDGF-AA) or treated with 10 ng/mL PDGF-AA for 1 hour (+PDGF-AA) as above (Fig. 3A; Table
223 S7). Immunoprecipitation with a previously validated Srsf3 antibody (Dennison et al., 2021)
224 successfully enriched for Srsf3 in UV-crosslinked cells (Fig. 3B). We detected 6,555 total eCLIP
225 peaks in protein-coding genes in the -PDGF-AA samples and 8,584 total peaks in the +PDGF-
226 AA samples (Table S8). Among the -PDGF-AA peaks, 3,727 (56.9%) were located in exons
227 (CDS) and 1,690 (25.8%) were located within introns, with the rest binding within 5' UTRs (768,
228 11.7%) and 3' UTRs (367, 5.60%) (Fig. 3C,D; Table S9). We observed substantial shifts in
229 Srsf3-bound regions upon PDGF-AA stimulation. Many more +PDGF-AA peaks were located
230 within exons (7,139, 83.2%), and less were located within introns (765, 8.91%), 5' UTRs (389,
231 4.53%) and 3' UTRs (287, 3.34%) (Fig. 3C,D; Table S9). Given that SR proteins are crucial for
232 exon definition and bind to exonic splicing enhancers to recruit and stabilize core splicing
233 machinery (Fu & Maniatis, 1990; Krainer et al., 1991; Zahler et al., 1993), we investigated Srsf3
234 binding around 5' and 3' splice sites in response to PDGFRα signaling. Consistent with the
235 results above and previous findings (Änkö et al., 2012), Srsf3 binding was enriched in exonic
236 regions, as opposed to intronic regions, surrounding the splice sites (Fig. 3E). There was
237 greater mean coverage of Srsf3 peaks in the +PDGF-AA condition versus the -PDGF-AA
238 condition within 100 nucleotides upstream of the 5' splice site and within 100 nucleotides
239 downstream of the 3' splice site (Fig. 3E). Additionally, we detected decreased mean coverage
240 in the +PDGF-AA condition within 25 nucleotides downstream of the 5' splice site boundary
241 (Fig. 3E). Taken together, these data show that PDGFRα signaling leads to increased binding of
242 Srsf3 to exons. Finally, we performed unbiased motif enrichment analysis of Srsf3 peaks in
243 unstimulated and PDGF-AA-treated samples, revealing that the mostly highly enriched motifs in
244 -PDGF-AA samples were CACACA and AAGAAG (Fig. 3F; Fig. S5). Of note, these CA-rich

245 motifs have previously been identified as canonical Srsf3 motifs in a CLIP study utilizing a stably
246 integrated SRSF3-EGFP transgene (Änkö et al., 2012). However, in PDGF-AA-stimulated
247 samples, the most highly enriched motifs were GAAGCG, GAAGAA, and AGAAGA (Fig. 3G;
248 Fig. S5), suggesting that PDGFRα signaling influences Srsf3 binding specificity.
249
250 *Srsf3 and PDGFRα signaling are associated with differential GC content and length of*
251 *alternatively-spliced exons*
252 We next probed our RNA-seq dataset to determine whether specific transcript features
253 were associated with Srsf3-dependent AS. When comparing significant AS events between
254 scramble and shSrsf3 samples in the absence of PDGF-AA stimulation, we found that included
255 exons had a significantly higher GC content (median value of 53.4%) than both skipped exons
256 (50.0%) and exons that were not differentially alternatively spliced (51.2%) when Srsf3 is
257 present (Fig. 4A, Table S10). Additionally, we observed that included exons had a significantly
258 lower ratio of downstream intron to exon GC content (0.856) than both skipped exons (0.901)
259 and exons that were not differentially alternatively spliced (0.888) in the presence of Srsf3 (Fig.
260 4B, Table S10). The same comparisons revealed that the ratio of upstream and downstream
261 intron to exon length was significantly decreased in included exons (median values of 12.4 and
262 10.6, respectively) as compared to both skipped exons (19.5 and 20.0) and exons that were not
263 differentially alternatively spliced (14.2 and 13.3) in the presence of Srsf3 (Fig. 4C,D, Table
264 S10). Taken together, our data demonstrate that exons which are included in the presence of
265 Srsf3 tend to have a higher GC content and lower intron to exon length ratio.
266 To determine whether PDGFRα signaling had an effect on the transcript features to
267 which Srsf3 bound, we subsequently examined our eCLIP dataset. We found that the exon GC
268 content was significantly increased in exons bound by Srsf3 in the absence of ligand treatment
269 (median value of 57.9%) as compared to unbound exons (51.5%) (Fig. 4E, Table S10).

270 However, exon GC content was similar between unbound exons and those bound by Srsf3
271 upon PDGF-AA stimulation (53.8%) (Fig. 4E, Table S10). These findings indicate that
272 PDGFRα signaling mediates binding of Srsf3 to exons with a lower GC content.
273
274 *Transcripts bound by Srsf3 that undergo alternative splicing upon PDGFRα signaling encode*
275 *regulators of PI3K signaling*
276 To determine which transcripts are directly bound by Srsf3 and subject to DE and/or AS,
277 we cross-referenced the eCLIP and RNA-seq datasets. We collated transcripts with an Srsf3
278 eCLIP peak that were uniquely detected in the -PDGF-AA or +PDGF-AA samples (2,660
279 transcripts across 3,388 peaks) (Tables S8 and S11). Similarly, we gathered differentially-
280 expressed genes (596) or differentially alternatively-spliced transcripts (985) uniquely found in
281 one of the four treatment comparisons (Fig. 5A, Table S11). Only 32 (5.4%) of the DE genes
282 were directly bound by Srsf3, while 233 (23.7%) of the alternatively-spliced transcripts had an
283 Srsf3 eCLIP peak, with very little overlap (1 transcript) between all three categories (Fig. 5A).
284 We next sought to identify high-confidence transcripts for which Srsf3 binding had an
285 increased likelihood of contributing to AS. Previous studies revealed enrichment of functional
286 RBP motifs near alternatively-spliced exons (Yee et al., 2019). As such, we correlated the
287 eCLIP peaks with AS events across all four treatment comparisons by identifying transcripts in
288 which Srsf3 bound within an alternatively-spliced exon or within 250 bp of the neighboring
289 introns (Tables S12-S15). In agreement with our findings above for the entire eCLIP dataset,
290 Srsf3 exhibited differential binding in exons and surrounding the 5' and 3' splice sites upon
291 PDGF-AA stimulation in these high-confidence, overlapping datasets (Fig. S6A,B). We
292 performed an unbiased motif enrichment analysis of Srsf3 peaks within the high-confidence,
293 overlapping datasets, again revealing different motifs between ligand treatment conditions and
294 an enrichment of GA-rich motifs in the +PDGF-AA samples (Fig. S6C,D).

295 To determine whether transcripts that are differentially bound by Srsf3 and undergo
296 differential AS downstream of PDGFRα signaling contribute to shared biological outputs, we
297 conducted GO analysis of the 149 unique transcripts from the high-confidence, overlapping
298 datasets. The most significant terms for biological process involved protein phosphorylation and
299 deacetylation, and RNA metabolism (Fig. 5B). Given that PI3K-mediated PDGFRα signaling is
300 critical for craniofacial development and regulates AS in this context (Dennison et al., 2021;
301 Fantauzzo & Soriano, 2014; Klinghoffer et al., 2002), we turned our focus toward GO terms
302 associated with this signaling pathway. We noted enrichment of PI3K-related GO terms (Fig.
303 5C), which encompassed the genes *Becn1, Wdr81* and *Acap3* (Fig. 5D). Related to their roles
304 in PI3K signaling, each of these gene products has been shown to regulate membrane and/or
305 endocytic trafficking. Phosphatidylinositol 3-phosphate (PI(3)P) is a critical component of early
306 endosomes and is mainly generated by conversion of phosphatidylinositol (PI) by the class III
307 PI3K complex, which includes Beclin-1 (encoded by *Becn1*) (Wallroth & Haucke, 2018). WDR81
308 and Beclin-1 have been shown to interact, resulting in decreased endosomal PI(3)P synthesis,
309 PI(3)P turnover and early endosome conversion to late endosomes (Liu et al., 2016).
310 Importantly, this role of WDR81 contributes to RTK degradation (Rapiteanu et al., 2016). Finally,
311 Acap3 is a GTPase-activating protein (GAP) for the small GTPase Arf6, converting Arf6 to an
312 inactive, GDP-bound state (Miura et al., 2016). Arf6 localizes to the plasma membrane and
313 endosomes, and has been shown to regulate endocytic membrane trafficking by increasing
314 PI(4,5)P2 levels at the cell periphery (D'Souza-Schorey and Chavrier, 2006). Further,
315 constitutive activation of Arf6 leads to upregulation of the gene encoding the p85 regulatory
316 subunit of PI3K and increased activity of both PI3K and AKT (Yoo et al., 2019).
317 Within our data, Srsf3 binding was increased in *Becn1* exon 7 upon PDGF-AA
318 stimulation, at an enriched motif within the high-confidence, overlapping datasets, and we
319 observed a corresponding increase in retention of adjacent intron 7 (Fig. 5D,E). As *Becn1* intron

320 7 contains a premature termination codon (PTC), this event is predicted to result in nonsense-
321 mediated decay (NMD) in the absence of Srsf3 (Fig. 5E). Srsf3 binding was also increased in
322 *Wdr81* exon 8 in response to PDGF-AA treatment, and our analyses revealed a corresponding
323 increase in excision of adjacent exon 9 (Fig. 5D,E). Because *Wdr81* exon 9 encodes two WD-
324 repeat domains, which are generally believed to form a β propellor structure required for protein
325 interactions (Li & Roberts, 2001), this AS event is predicted to result in a protein missing a
326 functional domain (Fig. 5E). These splicing patterns predict increased levels of Beclin-1 and
327 decreased levels of functional Wdr81 in the presence of Srsf3 and PDGF-AA stimulation,
328 resulting in augmented early endosome formation. Srsf3 binding was additionally increased in
329 *Acap3* exon 19 upon PDGF-AA stimulation, at an enriched motif within the high-confidence,
330 overlapping datasets, and we observed a corresponding increase in excision of adjacent intron
331 19 (Fig. 5D,E). As *Acap3* intron 19 contains a PTC, this event is predicted to result in more
332 transcripts encoding full-length protein (Fig. 5E).
333 Finally, as Wdr81 protein levels are predicted to regulate RTK trafficking between early
334 and late endosomes, we confirmed the differential AS of *Wdr81* transcripts between
335 unstimulated scramble cells and scramble cells treated with PDGF-AA ligand for 1 hour by
336 qPCR using primers within constitutively-expressed exons flanking alternatively-spliced exon 9.
337 This analysis revealed a decreased PSI for *Wdr81* in each of three biological replicates upon
338 PDGF-AA ligand treatment (Fig. 5F). Relatedly, we assessed the ratio of larger isoforms of
339 Wdr81 protein (containing the WD3 domain) to smaller isoforms (missing the WD3 domain) via
340 western blotting. Consistent with our RNA-seq and qPCR results, PDGF-AA stimulation for 24
341 hours in the presence of Srsf3 led to an increase in smaller Wdr81 protein isoforms (Fig. 5G).
342
343 *Srsf3 regulates early endosome size and phosphorylation of Akt downstream of PDGFRα*
344 *signaling*

345 Given that Srsf3 differentially binds to transcripts that encode proteins involved in early
346 endosomal trafficking downstream of PDGFRα signaling, we first examined the formation of
347 Rab5-positive early endosomes (Zerial & McBride, 2001) in response to a time course of PDGF-
348 AA ligand stimulation in scramble versus shSrsf3 cells. As expected, Rab5 puncta size
349 increased from 0 min ($9.79 \times 10^{-4} \pm 1.13 \times 10^{-4}$ arbitrary units; mean ± s.e.m.) to 15 min of ligand
350 stimulation ($2.01 \times 10^{-3} \pm 7.20 \times 10^{-4}$ arbitrary units) in scramble cells, and significantly so by 60
351 min ($2.58 \times 10^{-3} \pm 9.20 \times 10^{-4}$ arbitrary units) (Fig. 6A, C-C"', E-E"', G-G"'). However, this
352 increase was not observed in the absence of Srsf3 ($9.21 \times 10^{-4} \pm 1.61 \times 10^{-4}$ arbitrary units at 60
353 min) (Fig. 6A, D-D"', F-F"', H-H"'), demonstrating that Srsf3-mediated PDGFRα signaling leads
354 to enlarged early endosomes.
355 We next examined colocalization of PDGFRα with Rab5, as an estimate of receptor
356 levels in early endosomes. Colocalization levels increased from 0 min (0.332 ± 0.0832
357 Pearson's correlation coefficient (PCC); mean ± s.e.m.) to 15 min (0.429 ± 0.108 PCC) of
358 PDGF-AA treatment in scramble cells, then decreased to near baseline levels by 60 min (0.348
359 ± 0.0885 PCC) (Fig. 6B, C-C"', E-E"', G-G"') as a subset of PDGFRα homodimers are likely
360 trafficked to late endosomes (Rogers et al., 2022). Strikingly, shSrsf3 cells exhibited a
361 significant decrease in colocalization between PDGFRα and Rab5 by 60 min of ligand treatment
362 (0.186 ± 0.0102 PCC) (Fig. 6B, D-D"', F-F"', H-H"'), indicating that Srsf3 activity downstream of
363 PDGFRα signaling results in retention of PDGFRα in early endosomes.
364 Finally, we previously demonstrated that rapid internalization of PDGFRα homodimers
365 following PDGF-AA ligand stimulation is critical for downstream AKT phosphorylation (Rogers et
366 al., 2022). As such, we examined phospho-Akt levels as a readout of PDGFRα activation in
367 early endosomes. While PDGF-AA treatment for 15 min induced a robust phospho-Akt
368 response in scramble cells (13.5 ± 7.39 relative induction, mean ± s.e.m.) this response was
369 muted in shSrsf3 cells at the same timepoint (5.73 ± 1.91) (Fig. 6I). These findings further

370 suggest that retention of PDGFRα in early endosomes leads to increases in downstream PI3K-
371 mediated Akt signaling. Collectively, our data point to a feedback loop in which PI3K/Akt-
372 mediated PDGFRα signaling results in the nuclear translocation of Srsf3 and the subsequent
373 AS of transcripts to decrease levels of proteins that promote PDGFRα trafficking out of early
374 endosomes (Fig. 6J).
375
376 **Discussion**
377 In this study, we confirmed our prior *in vivo* results in the mouse embryonic facial
378 mesenchyme (Dennison et al., 2021) that PDGFRα signaling primary regulates gene expression
379 via AS. PDGF-AA-dependent differential gene expression was minimal following one hour of
380 ligand treatment and led to increased expression of immediate early genes *Klf10, Egf3* and
381 *Egr1*, consistent with previous findings (Vasudevan et al., 2015) and in line with the enriched
382 GO terms of regulation of transcription and DNA binding. Alternatively, PDGF-AA-dependent
383 alternatively-spliced transcripts were enriched for protein kinase activity, consistent with our
384 prior AS findings upon disruption of PI3K-mediated PDGFRα signaling in the palatal shelf
385 mesenchyme (Dennison et al., 2021). Importantly, our results demonstrated a significant
386 dependence on the RBP Srsf3 for AS downstream of PDGFRα activation. In fact, we found that
387 88% of Srsf3-dependent and 99% of PDGF-AA-dependent alternatively-spliced transcripts were
388 responsive to both Srsf3 activity and PDGFRα signaling. As discussed above, Srsf3 is
389 phosphorylated downstream of multiple stimuli (Bavelloni et al., 2014; Dennison et al., 2021;
390 Fantauzzo & Soriano, 2014; Long et al., 2019; Zhou et al., 2012), and it is likely that these
391 additional inputs contributed to Srsf3-dependent AS that was non-responsive to PDGF-AA
392 treatment. Further, our previous mass spectrometry screen identified 11 additional RBPs
393 involved in AS that are phosphorylated by Akt downstream of PI3K-mediated PDGFRα signaling
394 in primary MEPM cells (Fantauzzo & Soriano, 2014), which may account for the small fraction of

395 PDGF-AA-dependent AS that was non-responsive to Srsf3 knockdown. However, our RNA-seq
396 results together with the phenotypic overlap of embryos with neural crest-specific ablation of
397 *Srsf3* and mutant mouse models of *Pdgfra* and/or its ligands (Andrae et al., 2016; Dennison et
398 al., 2021; Ding et al., 2004; Fantauzzo & Soriano, 2014; Fredriksson et al., 2012; Klinghoffer et
399 al., 2002; Soriano, 1997) make a compelling case for Srsf3 serving as a critical effector of
400 PDGFRα signaling in the facial mesenchyme.

401 Here, we observed that Srsf3-dependent skipped exon events were enriched for
402 transcripts with a +ΔPSI (exon skipped more often in shSrsf3 samples) in the absence of PDGF-
403 AA stimulation, consistent with Srsf3 promoting exon inclusion. Alternatively, PDGF-AA ligand
404 treatment led to an increase in the percentage of Srsf3-dependent transcripts with a -ΔPSI
405 (exon included more often in shSrsf3 samples), suggesting that PDGFRα signaling causes
406 decreased exon inclusion in the presence of Srsf3. Interestingly, a recent paper found that
407 tethering Srsf3 downstream of the 5' splice site or upstream of the 3' splice site using MS2 stem
408 loops did not lead to AS of a splicing reporter (Schmok et al., 2024). However, the assay did not
409 test tethering within the exon and used a single minigene sequence context, and thus had the
410 potential to lead to false negative results (Schmok et al., 2024). Whether phosphorylation of
411 Srsf3 directly influences its binding to target RNAs or acts to modulate Srsf3 protein-protein
412 interactions which then contribute to differential RNA binding remains to be determined, though
413 findings from Schmok et al., 2024 may argue for the latter mechanism. Studies identifying
414 proteins that differentially interact with Srsf3 in response to PDGF-AA ligand stimulation are
415 ongoing and will shed light on these mechanisms.

416 This study represents the first endogenous CLIP analysis of Srsf3 in the absence of
417 protein tagging, and thus circumvents potential limitations with prior approaches in which
418 assayed RBPs were overexpressed and/or fused to another protein. Our eCLIP analyses
419 revealed several changes in Srsf3 transcript binding downstream of PDGF-AA stimulation,

420 including increased Srsf3 binding to exons and loss of Srsf3 binding to canonical CA-rich motifs.
421 A previous CLIP study using a stably integrated SRSF3-EGFP transgene in mouse P19 cells
422 determined that SRSF3 binding was enriched in exons, particularly within 100 nucleotides of the
423 5' and, to a lesser extent, 3' splice sites (Änkö et al., 2012), consistent with our results. This
424 same study identified a CA-rich canonical SRSF3 motif (Änkö et al., 2012). While such motifs
425 were identified here in the absence of PDGF-AA treatment, they were lost upon ligand
426 stimulation. Again, this shift could be due to loss of RNA binding owing to electrostatic repulsion
427 and/or changes in ribonucleoprotein composition and will be the subject of future studies.
428 Our findings additionally pointed to novel properties of exons whose inclusion is
429 dependent on Srsf3 in the absence of PDGFRα signaling. We demonstrated that these included
430 exons had a higher GC content, a lower ratio of downstream intron to exon GC content and a
431 decreased ratio of upstream and downstream intron to exon length. These findings are
432 consistent with previous results demonstrating that included exons tend to have higher GC
433 content than the flanking introns (Amit et al., 2012). Of note, PDGF-AA ligand stimulation
434 resulted in binding of Srsf3 to exons with a lower GC content, again suggesting that
435 phosphorylation of the RBP downstream of this signaling axis promotes exon skipping.
436 By cross-referencing our RNA-seq and eCLIP datasets, we showed that 24% of the
437 alternatively-spliced transcripts across our four treatment comparisons had an Srsf3 eCLIP
438 peak. As Srsf3 also has functions in the cytoplasm, such as RNA trafficking, translation and
439 degradation (Howard & Sanford, 2015), the additional eCLIP peaks may reflect alternate roles
440 for Srsf3 in RNA metabolism. Conversely, Srsf3-mediated AS may be delayed following
441 transcript binding in the short timeframe of our experimental design. However, the extent of
442 overlap that we observed is in line with previous studies correlating alternatively-spliced
443 transcripts upon knockdown of an RBP with endogenous eCLIP results for that same RBP,
444 including Rbfox2 (10%) (Moss et al., 2023) and LUC7L2 (18-26%) (Jourdain et al., 2021). The

445 degree to which our RNA-seq and eCLIP datasets overlapped here points to the robustness and
446 biological significance of our findings.

447 Our combined analyses demonstrated that Srsf3 binds and mediates the AS of
448 transcripts that encode proteins that regulate PI3K signaling and early endosomal trafficking
449 downstream of PDGFRα activation, including *Becn1, Wdr81* and *Acap3.* Homozygous missense
450 mutations in *WDR81* cause Cerebellar ataxia, impaired intellectual development, and
451 dysequilibrium syndrome 2 (OMIM 610185) in humans (Gulsuner et al., 2011), with some
452 patients exhibiting coarse facial features and strabismus (Garcias & Roth, 2007), pointing to a
453 critical role for this gene product in craniofacial development. Consistently, we found that related
454 GO terms, such as phosphatidylinositol phosphate binding and endosome to lysosome
455 transport, were significantly enriched among alternatively-spliced transcripts in murine
456 embryonic facial mesenchyme upon loss of PI3K binding to PDGFRα and/or knockdown of
457 *Srsf3* (Dennison et al., 2021). These data further confirm that our iMEPM model system served
458 as a powerful platform to uncover mechanisms that are utilized during craniofacial development
459 *in vivo*.

460 Our subsequent *in vitro* validation studies showed that Srsf3-mediated PDGFRα
461 signaling results in enlarged early endosomes, retention of the receptor in these early
462 endosomes and increased downstream PI3K-mediated Akt signaling. Relatedly, we and others
463 have linked spatial organization with the propagation of PDGFRα signaling, such that rapid
464 internalization of the receptors into early endosomes or autophagy of the receptors are required
465 for maximal phosphorylation of AKT downstream of PDGFRα activation (Rogers et al., 2022;
466 Simpson et al., 2024). Together, these results indicate a feedback loop at play in the
467 craniofacial mesenchyme in which stimulation of PDGFRα homodimer signaling leads to Srsf3-
468 dependent AS of transcripts, a subsequent increase in the levels of proteins that maintain the
469 receptor in early endosomes and a corresponding decrease in the levels of proteins that

470 promote trafficking of the receptor to late endosomes for eventual degradation. These findings
471 thus represent a novel mechanism by which PDGFRα activity is maintained and propagated
472 within the cell. Whether similar mechanisms exist downstream of alternate RTKs or contribute to
473 increases in the phosphorylation of effector proteins other than Akt remain to be determined. In
474 the future, it will be worthwhile to attempt to functionally link the AS of transcripts such as
475 *Becn1, Wdr81* and/or *Acap3* to the endosomal trafficking changes observed above using splice-
476 switching antisense oligonucleotides (ASOs).
477 Taken together, our findings significantly enhance our understanding of the molecular
478 mechanisms by which Srsf3 activity is regulated downstream of growth factor stimulation.
479 Interestingly, a recent study demonstrated that retention of another shuttling SR protein, Srsf1,
480 exclusively in the nucleus resulted in widespread ciliary defects in mice (Haward et al., 2021).
481 This finding indicates that dissecting nuclear from cytoplasmic functions of SR proteins can
482 provide powerful insight into the physiological relevance of each. Going forward, it will be critical
483 to explore the *in vivo* consequences of abrogating Akt-mediated phosphorylation of Srsf3 and
484 comparing the resulting phenotype to those of embryos with constitutive or conditional ablation
485 of *Srsf3* in the neural crest lineage (Dennison et al., 2021; Jumaa et al., 1999). These
486 experiments are ongoing and should shed considerable light on the roles of RBP post-
487 translational modifications during development.
488

489 **Materials and Methods**

490 *Generation of scramble and* Srsf3 *shRNA iMEPM cell lines*

491 Immortalized mouse embryonic palatal mesenchyme (iMEPM) cells were derived from a
492 male *Cdkn2a*$^{-/-}$ embryo as previously described (Fantauzzo & Soriano, 2017). iMEPM cells were
493 cultured in growth medium [Dulbecco's modified Eagle's medium (Gibco, Thermo Fisher
494 Scientific, Waltham, MA, USA) supplemented with 50 U/mL penicillin (Gibco), 50 μg/mL

495 streptomycin (Gibco) and 2 mM L-glutamine (Gibco) containing 10% fetal bovine serum (FBS)
496 (Hyclone Laboratories Inc., Logan, UT, USA)] and grown at 37°C in 5% carbon dioxide. iMEPM
497 cells were tested for mycoplasma contamination using the MycoAlert Mycoplasma Detection Kit
498 (Lonza Group Ltd, Basel, Switzerland). Packaged lentiviruses containing pLV[shRNA]-
499 EGFP:T2A:Puro-U6>Scramble_shRNA (vectorID: VB010000-0009mxc) with sequence
500 CCTAAGGTTAAGTCGCCCTCGCTCGAGCGAGGGCGACTTAACCTTAGG or pLV[shRNA]-
501 EGFP:T2A:Puro-U6>mSrsf3[shRNA#1] (vectorID: VB900060-7699yyh) with sequence
502 GAATGATAAAGCGGTGTTTACTCGAGTAAACACCGCTTTATCATTCC were purchased from
503 VectorBuilder (Chicago, IL, USA). Medium containing lentivirus for a multiplicity of infection of
504 10 for 200,000 cells with the addition of 10 ug/mL polybrene was added to iMEPM cells for 16 h,
505 and cells were subsequently grown in the presence of 4 ug/mL puromycin for 10 days. Cells
506 with the highest GFP expression (top 20%) were isolated on a Moflo XDP 100 cell sorter
507 (Beckman Coulter Inc., Brea, CA, USA) and expanded. Srsf3 expression in scramble and *Srsf3*
508 shRNA cell lines was confirmed by western blotting. Once the stable cell lines were established,
509 they were split at a ratio of 1:4 for maintenance. Scramble and *Srsf3* shRNA cells were used for
510 experiments at passages 9-20.
511
512 *Immunoprecipitation and western blotting*
513 To induce PDGFRα signaling, cells at ~70% confluence were serum starved for 24 h in
514 starvation medium [Dulbecco's modified Eagle's medium (Gibco) supplemented with 50 U/mL
515 penicillin (Gibco), 50 μg/mL streptomycin (Gibco) and 2 mM L-glutamine (Gibco) containing
516 0.1% FBS (Hyclone Laboratories Inc.)] and stimulated with 10 ng/mL rat PDGF-AA ligand (R&D
517 Systems, Minneapolis, MN, USA) diluted from a 1.5 μg/mL working solution in 40 nM HCl
518 containing 0.1% BSA for the indicated length of time. When applicable, UV-crosslinking was
519 performed at 254 nm and 400 mJ/cm^2 using a Vari-X-Link system (UVO3 Ltd, Cambridgeshire,

520 UK). For immunoprecipitation of Srsf3, cells were resuspended in ice-cold CLIP lysis buffer [50
521 mM Tris-HCl pH 7.4, 100 mM NaCl, 1% NP-40, 0.1% SDS, 0.5% sodium deoxycholate, 1x
522 complete Mini protease inhibitor cocktail (Roche, MilliporeSigma, Burlington, MA, USA), 1 mM
523 PMSF, 10 mM NaF, 1 mM Na_3VO_4, 25 mM β-glycerophosphate]. Cleared lysates were collected
524 by centrifugation at 18,000 *g* for 20 min at 4°C. Anti-Srsf3 antibody (10 μg/sample) (ab73891,
525 Abcam, Waltham, MA, USA) was added to protein A Dynabeads (125 μL/sample) (Thermo
526 Fisher Scientific) washed twice in ice-cold CLIP lysis buffer and incubated for 45 min at room
527 temperature. Cells lysates were incubated with antibody-conjugated Dynabeads or Dynabeads
528 M-280 sheep anti-rabbit IgG (Thermo Fisher Scientific) washed twice in ice-cold CLIP lysis
529 buffer overnight at 4°C. The following day, Dynabeads were washed twice each with ice-cold
530 high salt wash buffer [50 mM Tris-HCl pH 7.4, 1M NaCl, 1 mM EDTA, 1% NP-40, 0.1% SDS,
531 0.5% sodium deoxycholate] followed by ice-cold wash buffer [20 mM Tris-HCl pH 7.4, 10 mM
532 $MgCl_2$, 0.2% Tween-20]. The precipitated proteins were eluted with 1x NuPAGE LDS buffer
533 (Thermo Fisher Scientific) containing 100 mM dithiothreitol, heated for 10 minutes at 70°C, and
534 separated by SDS-PAGE. For western blotting of whole-cell lysates, protein lysates were
535 generated by resuspending cells in ice-cold NP-40 lysis buffer (20 mM Tris-HCl pH 8, 150 mM
536 NaCl, 10% glycerol, 1% Nonidet P-40, 2 mM EDTA, 1x complete Mini protease inhibitor cocktail
537 (Roche), 1 mM PMSM, 10 mM NaF, 1 mM Na_3VO_4, 25 mM β-glycerophosphate) and collecting
538 cleared lysates by centrifugation at 13,400 *g* at 4°C for 20 min. Laemmli buffer containing 10%
539 β-mercaptoethanol was added to the lysates, which were heated for 5 min at 100°C. Proteins
540 were subsequently separated by SDS-PAGE. Western blot analysis was performed according to
541 standard protocols using horseradish peroxidase-conjugated secondary antibodies. Blots were
542 imaged using a ChemiDoc XRS+ (Bio-Rad Laboratories, Inc., Hercules, CA, USA) or a
543 ChemiDoc (Bio-Rad Laboratories, Inc.). The following primary antibodies were used for western
544 blotting: Srsf3 (1:1,000, ab73891, Abcam), Gapdh (1:50,000, 60004, Proteintech Group, Inc.,

545 Rosemont, IL, USA), Wdr81 (1:1,000, 24874-1-AP, Proteintech Group, Inc.), phospho-Akt
546 (Ser473) (1:1,000, 9271, Cell Signaling Technology, Inc., Danvers, MA, USA), Akt (1:1,000,
547 9272, Cell Signaling Technology, Inc.), horseradish peroxidase-conjugated goat anti-mouse IgG
548 (1:20,000, 115035003, Jackson ImmunoResearch Inc., West Grove, PA, USA), horseradish
549 peroxidase-conjugated goat anti-rabbit IgG (1:20,000, 111035003;, Jackson ImmunoResearch
550 Inc.). Quantifications of signal intensity were performed with ImageJ software (version 1.53t,
551 National Institutes of Health, Bethesda, MD, USA). The relative ratio of Wdr81 isoforms was
552 calculated as the fraction of the larger isoform divided by the fraction of the smaller isoform
553 following normalization to Gapdh levels. Relative phospho-Akt levels were determined by
554 normalizing to total Akt levels. When applicable, statistical analyses were performed with Prism
555 10 (GraphPad Software Inc., San Diego, CA, USA) using a two-tailed, ratio paired *t*-test within
556 each cell line and a two-tailed, unpaired *t*-test with Welch's correction between each cell line.
557 Immunoprecipitation and western blotting experiments were performed across three
558 independent experiments.
559
560 *RNA-sequencing and related bioinformatics analyses*
561 8×10^5 cells obtained from each of three independent biological replicates per treatment
562 were frozen on liquid nitrogen and stored at -80°C. Following thawing, total RNA was
563 simultaneously isolated from all samples using the RNeasy Mini Kit (Qiagen, Inc., Germantown,
564 MD, USA) according to the manufacturer's instructions. RNA was forwarded to the University of
565 Colorado Cancer Center Genomics Shared Resource for quality control, library preparation, and
566 sequencing. RNA purity, quantity and integrity were assessed with a NanoDrop (Thermo Fisher
567 Scientific) and a 4200 TapeStation System (Agilent Technologies, Inc., Santa Clara, CA, USA)
568 prior to library preparation. Total RNA (200 ng) was used for input into the Universal Plus
569 mRNA-Seq kit with NuQuant (Tecan Group Ltd., Männedorf, Switzerland). Dual index, stranded

570 libraries were prepared and sequenced on a NovaSeq 6000 Sequencing System (Illumina, San
571 Diego, CA, USA) to an average depth of ~54 million read pairs (2x150 bp reads).
572 Raw sequencing reads were de-multiplexed using bcl2fastq (Illumina). Trimming, filtering
573 and adapter contamination removal was performed using BBDuk (from the BBmap v35.85 tool
574 suite) (Bushnell, 2015). For differential expression analysis, transcript abundance was quantified
575 using Salmon (v1.4.0) (Patro et al., 2017) and a decoy-aware transcriptome index prepared
576 using GENCODE (Frankish et al., 2019) GRCm39 M26. Gene level summaries were calculated
577 using tximport (Soneson et al., 2016) in R and differential expression was measured using
578 DESeq2 (v.1.32.0) (Love et al., 2014). Significant changes in gene-level expression are
579 reported for cases with adjusted $P \leq 0.05$ and fold change $|FC| \geq 2$. Spearman correlation was
580 computed between conditions for differentially-expressed genes. For alternative splicing
581 analysis, raw FASTQ were trimmed to a uniform length of 125 bp. Reads were aligned to the
582 mouse genome (GRCm39 Gencode M26) using STAR (v.2.7.9a) (Dobin et al., 2013). Additional
583 parameters for STAR: --outFilterType BySJout --outFilterMismatchNmax 10 --
584 outFilterMismatchNoverLmax 0.04 --alignEndsType EndToEnd --runThreadN 16 --
585 alignSJDBoverhangMin 4 --alignIntronMax 300000 --alignSJoverhangMin 8 --alignIntronMin 20.
586 All splice junctions detected in at least 1 read from the first pass alignment were used in a
587 second pass alignment, per software documentation. Alternative splicing events were detected
588 using rMATS (v4.0.2, default parameters plus '—cstat 0.0001') (Shen et al. 2014). Reads
589 mapping to the splice junction as well as those mapping to the exon body were used in
590 downstream analyses. Detected events were compared between treatment groups and
591 considered significant with false discovery rate (FDR) ≤ 0.05, a difference in percent spliced in
592 ($|\Delta PSI|$) ≥ 0.05 and event detection in at least 10 reads in either condition. Raw read pairs,
593 trimmed read pairs for Salmon input, Salmon mapping rate per sample, trimmed read pairs (125
594 bp) for STAR input and STAR unique mapping rate can be found in Table S1. Gene ontology

595 analysis was performed with various libraries from the Enrichr gene list enrichment analysis tool
596 (Chen et al., 2013; Kuleshov et al., 2016) and terms with $P < 0.05$ were considered significant.
597
598 *qPCR*
599 Total RNA was isolated using the RNeasy mini kit (Qiagen, Germantown, MD, USA)
600 according to the manufacturer's instructions. First-strand cDNA was synthesized using a ratio of
601 2:1 random primers:oligo (dT) primer and SuperScript II RT (Invitrogen, Thermo Fisher
602 Scientific) according to the manufacturer's instructions. All reactions were performed with 1×
603 ThermoPol buffer [0.02 M Tris (pH 8.8), 0.01 M KCl, 0.01 M $(NH_4)_2SO_4$, 2 mM $MgSO_4$ and 0.1%
604 Triton X-100], 200 μM dNTPs, 200 nM primers (Integrated DNA Technologies, Inc., Coralville,
605 IA, USA), 0.6 U Taq polymerase and 1 μg cDNA in a 25 μL reaction volume. The primers used
606 can be found in Table S16. The following PCR protocol was used for *Arhgap12*: step1, 3 min at
607 94°C; step 2, 30 s at 94°C; step 3, 30 s at 47°C; step 4, 30 s at 72°C; repeat steps 2-4 for 34
608 cycles; and step 5, 5 min at 72°C. The following PCR protocol was used for *Cep55*: step1, 3 min
609 at 94°C; step 2, 30 s at 94°C; step 3, 30 s at 48°C; step 4, 30 s at 72°C; repeat steps 2-4 for 34
610 cycles; and step 5, 5 min at 72°C. Two-thirds of total PCR products were electrophoresed on a
611 2% agarose/TBE gel containing ethidium bromide and photographed on an Aplegen Omega
612 Fluor Gel Documentation System (Aplegen Inc., Pleasanton, CA, USA). Quantifications of band
613 intensity were performed with ImageJ software (version 1.53t, National Institutes of Health). The
614 following PCR protocol was used for *Wdr81*: step1, 3 min at 94°C; step 2, 30 s at 94°C; step 3,
615 30 s at 50°C; step 4, 30 s at 72°C; repeat steps 2-4 for 24 cycles; and step 5, 2 min at 72°C.
616 PCR products were purified with AMPure XP Reagent (Beckman Coulter, Brea, CA, USA) and
617 analyzed on a 4150 TapeStation System (Agilent Technologies, Inc.) using High Sensitivity
618 D1000 ScreenTape (Agilent Technologies, Inc.). The PSI was calculated independently for each
619 sample as the percentage of the larger isoform divided by the total abundance of all isoforms
620 within the given gel lane or TapeStation sample. Statistical analyses were performed with Prism

621 10 (GraphPad Software) using a two-tailed, unpaired *t*-test with Welch's correction. qPCR
622 reactions were performed using three biological replicates.
623
624 *Enhanced UV-crosslinking and immunoprecipitation and related bioinformatics analyses*
625 Experiments were performed as previously described in biological duplicates (Van
626 Nostrand et al., 2016, 2017). Briefly, 2 million cells per treatment were serum starved and
627 treated with 10 ng/mL PDGF-AA as described above. Cells were subsequently UV-crosslinked
628 at 254 nm and 400 mJ/cm^2, scraped in 1x phosphate buffered saline (PBS) and transferred to
629 1.5 mL Eppendorf tubes, at which point excess PBS was removed and cells were frozen on
630 liquid nitrogen and stored at -80°C. Following thawing, cells were lysed in ice-cold CLIP lysis
631 buffer, sonicated by BioRuptor (Diagenode, Denville, NJ, USA) and treated with RNase I
632 (Thermo Fisher Scientific). 2% of lysates were set aside as size-matched input samples. Srsf3-
633 RNA complexes were immunoprecipitated with anti-Srsf3 antibody (10 μg per sample)
634 (ab73891, Abcam) conjugated to protein A Dynabeads (Thermo Fisher Scientific). IP samples
635 were washed and dephosphorylated with FastAP (New England Biolabs, Ipswich, MA, USA)
636 and T4 PNK (New England Biolabs). IP samples underwent on-bead ligation of barcoded RNA
637 adapters (/5phos/rArGrArUrCrGrGrArArGrArGrCrGrUrCrGrUrG/3SpC3/) to the 3' end using T4
638 RNA ligase (New England Biolabs). Following elution, protein-RNA complexes were run on 4-
639 12% Bis-Tris 1.5 mm gels (Thermo Fisher Scientific) and transferred onto nitrocellulose
640 membranes. The 20-75 kDa region was excised and digested with proteinase K (New England
641 Biolabs). RNA was isolated with acid phenol/chloroform/isoamyl alcohol (pH 6.5) (Thermo
642 Fisher Scientific), reverse transcribed with Superscript III (Thermo Fisher Scientific) and treated
643 with ExoSAP-IT (Affymetrix, Thermo Fisher Scientific) to remove excess primers and
644 unincorporated nucleotides. Samples underwent 3' ligation of barcoded DNA adapters
645 (/5Phos/NNNNNNNNNNAGATCGGAAGAGCACACGTCTG/3SpC3/), clean-up with Dynabeads
646 MyOne Silane (Thermo Fisher Scientific) and qPCR to determine the appropriate number of

647 PCR cycles. Libraries were then amplified with Q5 PCR mix (New England Biolabs) for a total of
648 16-25 cycles. Libraries were forwarded to the University of Colorado Cancer Center Genomics
649 Shared Resource for quality control and sequencing. Sample integrity was assessed with a
650 D1000 ScreenTape System (Agilent Technologies, Inc.) and sequenced on a NovaSeq 6000
651 Sequencing System (Illumina) to an average depth of ~20 million read pairs (2x150 bp reads).
652 Raw sequencing reads were de-multiplexed using bcl2fastq (Illumina). Adapters were
653 trimmed using cutadapt (v.1.18) (Martin, 2011). Trimmed reads were quality filtered and
654 collapsed using a combination of FASTX-Toolkit (v.0.0.14)
655 (http://hannonlab.cshl.edu/fastx_toolkit), seqtk (v.1.3-r106) (https://github.com/lh3/seqtk) and
656 custom scripts. After collapsing the reads, unique molecular identifiers were removed using
657 seqtk. STAR index for repetitive elements was created using repetitive sequences from
658 msRepDB (Liao et al., 2022). Reads ≥ 18 nt were mapped to the repetitive elements using
659 STAR (v.2.7.9a) (Dobin et al. 2013). Reads unmapped to the repetitive elements were mapped
660 to the mouse genome (GRCm39 Gencode M26) using STAR (v.2.7.9a) with parameters
661 alignEndsType: EndtoEnd and outFilterMismatchNoverReadLmax: 0.04. Peaks were called
662 using omniCLIP (v.0.20) (Drewe-Boss et al., 2018) with the foreground penalty (--fg_pen)
663 parameter set to 5. Peaks were annotated and motif analyses performed using RCAS (v.1.19.0)
664 (Uyar et al., 2017) and custom R script. Motif enrichment significance was calculated using a *t*-
665 test. For visualization purposes, bigWig files were created from bam files using deepTools
666 (v.3.5.5) (Ramírez et al., 2016). Peaks were visualized in Integrative Genomics Viewer
667 (v.2.13.0) (Robinson et al., 2011). Intron and exon features were calculated using Matt (v.1.3.1)
668 (Gohr & Irimia, 2019), and statistical analyses were performed using a Mann-Whitney U test.
669 For overlap of eCLIP peaks and alternative splicing events, peak coordinates were taken from
670 omniCLIP bed files and alternative splicing coordinates were taken from rMATS output.
671 Overlapping coordinates from alternative splicing events were defined following the rMAPS
672 default values (Park et al., 2016). Overlap was calculated using valr (v.0.6.4) (Riemondy et al.,

673 2017) and custom R scripts. Raw read pairs, trimmed read pairs, collapsed reads, reads after
674 removing repetitive elements, mapped reads, peaks and annotated peaks can be found in Table
675 S7. Gene ontology analysis was performed with various libraries from the Enrichr gene list
676 enrichment analysis tool (Chen et al., 2013; Kuleshov et al., 2016) and terms with $P < 0.05$ were
677 considered significant.
678
679 *Immunofluorescence analysis*
680 Cells were seeded onto glass coverslips at ~40% confluency per 24-well plate well in
681 iMEPM growth medium. After 24 h, cells were serum starved and treated with 10 ng/mL PDGF-
682 AA as described above. Cells were fixed in 4% paraformaldehyde (PFA) in PBS with 0.1%
683 Triton X-100 for 10 min and washed in PBS. Cells were blocked for 1 h in 5% normal donkey
684 serum (Jackson ImmunoResearch Inc.) in PBS and incubated overnight at 4°C in primary
685 antibody diluted in 1% normal donkey serum in PBS. After washing in PBS, cells were
686 incubated in Alexa Fluor 488-conjugated donkey anti-rabbit secondary antibody (1:1,000;
687 A21206; Invitrogen) or Alexa Fluor 546-conjugated donkey anti-mouse secondary antibody
688 (1:1,000; A10036; Invitrogen) diluted in 1% normal donkey serum in PBS with 2 µg/ml DAPI
689 (Sigma-Aldrich, St. Louis, MO, USA) for 1 h. Cells were mounted in VECTASHIELD HardSet
690 Antifade Mounting Medium (Vector Laboratories, Inc., Burlingame, CA, USA) and photographed
691 using an Axiocam 506 mono digital camera (Carl Zeiss Microscopy LLC, White Plains, NY,
692 USA) fitted onto an Axio Observer 7 fluorescence microscope (Carl Zeiss Microscopy LLC) with
693 the 63x oil objective with a numerical aperture of 1.4 at room temperature. The following
694 antibodies were used for immunofluorescence analysis: Rab5 (1:200, C8B1, 3547, Cell
695 Signaling Technology Inc.), PDGFRα (1:20, AF1062, R&D Systems). For assessment of Rab5
696 puncta size and colocalization experiments, three independent trials, or biological replicates,
697 were performed. For each biological replicate, 20 technical replicates consisting of individual
698 cells were imaged with Z-stacks (0.24 µm between Z-stacks with a range of 1–6 Z-stacks) per

699 timepoint. Images were deconvoluted using ZEN Blue software (Carl Zeiss Microscopy LLC)
700 using the 'Better, fast (Regularized Inverse Filter)' setting. Extended depth of focus was applied
701 to Z-stacks using ZEN Blue software (Carl Zeiss Microscopy LLC) to generate images with the
702 maximum depth of field. For assessment of Rab5 puncta size, images were converted to 8-bit
703 using Fiji software (version 2.14.0/1.54f). Images were subsequently converted to a mask and
704 watershed separation was applied. A region of interest (ROI) was drawn around each Rab5-
705 positive cell and particles were analyzed per cell using the "analyze particles" function. For
706 colocalization measurements, an ROI was drawn around each PDGFRα-positive cell in the
707 corresponding Cy3 (marker) channel using Fiji. For each image with a given ROI, the Cy3
708 channel and the EGFP channel were converted to 8-bit images. Colocalization was measured
709 using the Colocalization Threshold function, where the rcoloc value [Pearson's correlation
710 coefficient (PCC)] was used in statistical analysis. Statistical analyses were performed on the
711 average values from each biological replicate with Prism 10 (GraphPad Software Inc.) using a
712 two-way ANOVA followed by uncorrected Fisher's LSD test.
713

714 **Acknowledgements**

715 We are grateful to Jessica Johnston and Erin Binne for technical assistance, and Drs. Allison
716 Swain, Justin Roberts and Aaron Johnson at the University of Colorado Anschutz Medical
717 Campus for advice on eCLIP experiments. Cell sorting was performed at the University of
718 Colorado Cancer Center Flow Cytometry Shared Resource with assistance from Dr. Dmitry
719 Baturin. RNA-seq and eCLIP sequencing experiments were performed at the University of
720 Colorado Cancer Center Genomics Shared Resource. We thank members of the Fantauzzo
721 laboratory for their critical comments on the manuscript.
722

723 **Competing Interests**

724 The authors declare no competing or financial interests.

725

726 **Author contributions**

727 Conceptualization: TEF, MS, NM, KAF; Methodology: TEF, MS, NM, KAF; Formal analysis:
728 TEF, MS, EDL, KAF; Investigation: TEF, MS, EDL; Writing – Original Draft: TEF, KAF; Writing –
729 Review & Editing: MS, EDL, NM; Visualization: TEF, MS, KAF; Supervision: NM, KAF; Project
730 administration: KAF; Funding acquisition: TEF, KAF.

731

732 **Funding**

733 This work was supported by National Institutes of Health grants R01DE030864 (to K.A.F.),
734 R35GM147025 (to N.M.), the University of Colorado Anschutz Medical Campus RNA
735 Bioscience Initiative (to N.M. and M.P.S.) and F31DE032252 (to T.E.F.). The Flow Cytometry
736 Shared Resource and Genomics Shared Resource are supported by National Institutes of
737 Health grant P30CA046934.

738

739 **Data Availability**

740 The eCLIP and RNA-sequencing datasets generated during this study have been deposited in
741 GEO under SuperSeries accession number GSE263170. Custom analysis scripts will be
742 provided by Dr. Larson through GitHub.

743

744 **References**

745 Akerman, M., David-Eden, H., Pinter, R. Y., & Mandel-Gutfreund, Y. (2009). A computational
746 approach for genome-wide mapping of splicing factor binding sites. *Genome Biology*,
747 *10*(3), R30. https://doi.org/10.1186/gb-2009-10-3-r30

748 Amit, M., Donyo, M., Hollander, D., Goren, A., Kim, E., Gelfman, S., Lev-Maor, G., Burstein, D.,
749 Schwartz, S., Postolsky, B., Pupko, T., & Ast, G. (2012). Differential GC Content

750 between Exons and Introns Establishes Distinct Strategies of Splice-Site Recognition.
751 *Cell Reports*, *1*(5), 543–556. https://doi.org/10.1016/j.celrep.2012.03.013
752 Andrae, J., Gouveia, L., Gallini, R., He, L., Fredriksson, L., Nilsson, I., Johansson, B. R.,
753 Eriksson, U., & Betsholtz, C. (2016). A role for PDGF-C/PDGFRα signaling in the
754 formation of the meningeal basement membranes surrounding the cerebral cortex.
755 *Biology Open*, *5*(4), 461–474. https://doi.org/10.1242/bio.017368
756 Änkö, M.-L., Müller-McNicoll, M., Brandl, H., Curk, T., Gorup, C., Henry, I., Ule, J., &
757 Neugebauer, K. M. (2012). The RNA-binding landscapes of two SR proteins reveal
758 unique functions and binding to diverse RNA classes. *Genome Biology*, *13*(3), R17.
759 https://doi.org/10.1186/gb-2012-13-3-r17
760 Bavelloni, A., Piazzi, M., Faenza, I., Raffini, M., D'Angelo, A., Cattini, L., Cocco, L., & Blalock,
761 W. L. (2014). Prohibitin 2 represents a novel nuclear AKT substrate during all- *trans*
762 retinoic acid–induced differentiation of acute promyelocytic leukemia cells. *The FASEB*
763 *Journal*, *28*(5), 2009–2019. https://doi.org/10.1096/fj.13-244368
764 Bebee, T. W., Park, J. W., Sheridan, K. I., Warzecha, C. C., Cieply, B. W., Rohacek, A. M.,
765 Xing, Y., & Carstens, R. P. (2015). The splicing regulators Esrp1 and Esrp2 direct an
766 epithelial splicing program essential for mammalian development. *eLife*, *4*, e08954.
767 https://doi.org/10.7554/eLife.08954
768 Bushnell, B. (2015). *BBMap*. Https://Sourceforge.Net/Projects/Bbmap/.
769 https://sourceforge.net/projects/bbmap/
770 Chen, E. Y., Tan, C. M., Kou, Y., Duan, Q., Wang, Z., Meirelles, G. V., Clark, N. R., & Ma'ayan,
771 A. (2013). Enrichr: Interactive and collaborative HTML5 gene list enrichment analysis
772 tool. *BMC Bioinformatics*, *14*, 128. https://doi.org/10.1186/1471-2105-14-128
773 Choi, S. J., Marazita, M. L., Hart, P. S., Sulima, P. P., Field, L. L., McHenry, T. G., Govil, M.,
774 Cooper, M. E., Letra, A., Menezes, R., Narayanan, S., Mansilla, M. A., Granjeiro, J. M.,
775 Vieira, A. R., Lidral, A. C., Murray, J. C., & Hart, T. C. (2009). The PDGF-C regulatory

region SNP rs28999109 decreases promoter transcriptional activity and is associated with CL/P. *European Journal of Human Genetics*, *17*(6), 774–784. https://doi.org/10.1038/ejhg.2008.245

Cibi, D. M., Mia, M. M., Guna Shekeran, S., Yun, L. S., Sandireddy, R., Gupta, P., Hota, M., Sun, L., Ghosh, S., & Singh, M. K. (2019). Neural crest-specific deletion of Rbfox2 in mice leads to craniofacial abnormalities including cleft palate. *eLife*, *8*, e45418. https://doi.org/10.7554/eLife.45418

D'Souza-Schorey, C., & Chavrier, P. (2006). ARF proteins: roles in membrane traffic and beyond. *Nature Reviews Molecular Cell Biology*, *7*(5), 347-358. https://doi.org/10.1038/nrm1910

Dennison, B. J. C., Larson, E. D., Fu, R., Mo, J., & Fantauzzo, K. A. (2021). Srsf3 mediates alternative RNA splicing downstream of PDGFRα signaling in the facial mesenchyme. *Development*, *148*(14), dev199448. https://doi.org/10.1242/dev.199448

Ding, H., Wu, X., Boström, H., Kim, I., Wong, N., Tsoi, B., O'Rourke, M., Koh, G. Y., Soriano, P., Betsholtz, C., Hart, T. C., Marazita, M. L., Field, L. L., Tam, P. P. L., & Nagy, A. (2004). A specific requirement for PDGF-C in palate formation and PDGFR-α signaling. *Nature Genetics*, *36*(10), 1111–1116. https://doi.org/10.1038/ng1415

Dobin, A., Davis, C. A., Schlesinger, F., Drenkow, J., Zaleski, C., Jha, S., Batut, P., Chaisson, M., & Gingeras, T. R. (2013). STAR: ultrafast universal RNA-seq aligner. *Bioinformatics, 29*(1), 15-21. https://doi.org/10.1093/bioinformatics/bts635

Drewe-Boss, P., Wessels, H.-H., & Ohler, U. (2018). omniCLIP: Probabilistic identification of protein-RNA interactions from CLIP-seq data. *Genome Biology*, *19*(1), 183. https://doi.org/10.1186/s13059-018-1521-2

799 Fantauzzo, K. A., & Soriano, P. (2014). PI3K-mediated PDGFR signaling regulates survival and
800 proliferation in skeletal development through p53-dependent intracellular pathways.
801 *Genes & Development*, *28*(9), 1005–1017. https://doi.org/10.1101/gad.238709.114
802 Fantauzzo, K. A., & Soriano, P. (2017). Generation of an immortalized mouse embryonic palatal
803 mesenchyme cell line. *PLOS ONE*, *12*(6), e0179078.
804 https://doi.org/10.1371/journal.pone.0179078
805 Forman, T. E., Dennison, B. J. C., & Fantauzzo, K. A. (2021). The Role of RNA-Binding Proteins
806 in Vertebrate Neural Crest and Craniofacial Development. *Journal of Developmental*
807 *Biology*, *9*(3), 34. https://doi.org/10.3390/jdb9030034
808 Frankish, A., Diekhans, M., Ferreira, A. M., Johnson, R., Jungreis, I., Loveland, J., Mudge, J.
809 M., Sisu, C., Wright, J., Armstrong, J., Barnes, I., Berry, A., Bignell, A., Carbonell Sala,
810 S., Chrast, J., Cunningham, F., Di Domenico, T., Donaldson, S., Fiddes, I. T., … Flicek,
811 P. (2019). GENCODE reference annotation for the human and mouse genomes. *Nucleic*
812 *Acids Research*, *47*(D1), D766-763. https://doi.org/10.1093/nar/gky955
813 Fredriksson, L., Nilsson, I., Su, E. J., Andrae, J., Ding, H., Betsholtz, C., Eriksson, U., &
814 Lawrence, D. A. (2012). Platelet-Derived Growth Factor C Deficiency in C57BL/6 Mice
815 Leads to Abnormal Cerebral Vascularization, Loss of Neuroependymal Integrity, and
816 Ventricular Abnormalities. *The American Journal of Pathology*, *180*(3), 1136–1144.
817 https://doi.org/10.1016/j.ajpath.2011.12.006
818 Fu, X.-D., & Ares, M. (2014). Context-dependent control of alternative splicing by RNA-binding
819 proteins. *Nature Reviews Genetics*, *15*(10), 689–701. https://doi.org/10.1038/nrg3778
820 Fu, X.-D., & Maniatis, T. (1990). Factor required for mammalian spliceosome assembly is
821 localized to discrete regions in the nucleus. *Nature*, *343*(6257), 437–441.
822 https://doi.org/10.1038/343437a0

823 Garcias, G. D. L., & Roth, M. D. G. M. (2007). A Brazilian family with quadrupedal gait, severe
824 mental retardation, coarse facial characteristics, and hirsutism. *International Journal of*
825 *Neuroscience*, *117*(7), 927–933. https://doi.org/10.1080/00207450600910721
826 Gohr, A., & Irimia, M. (2019). *Matt*: Unix tools for alternative splicing analysis. *Bioinformatics*,
827 *35*(1), 130–132. https://doi.org/10.1093/bioinformatics/bty606
828 Gulsuner, S., Tekinay, A. B., Doerschner, K., Boyaci, H., Bilguvar, K., Unal, H., Ors, A., Onat, O.
829 E., Atalar, E., Basak, A. N., Topaloglu, H., Kansu, T., Tan, M., Tan, U., Gunel, M., &
830 Ozcelik, T. (2011). Homozygosity mapping and targeted genomic sequencing reveal the
831 gene responsible for cerebellar hypoplasia and quadrupedal locomotion in a
832 consanguineous kindred. *Genome Research*, *21*(12), 1995-2003.
833 https://doi.org/10.1101/gr.126110.111
834 Haward, F., Maslon, M. M., Yeyati, P. L., Bellora, N., Hansen, J. N., Aitken, S., Lawson, J., von
835 Kriegsheim, A., Wachten, D., Mill, P., Adams, I. R., & Caceres, J. F. (2021). Nucleo-
836 cytoplasmic shuttling of splicing factor SRSF1 is required for development and cilia
837 function. *eLife*, *10*, e65104. https://doi.org/10.7554/eLife.65104
838 He, F., & Soriano, P. (2013). A critical role for PDGFRα signaling in medial nasal process
839 development. *PLoS Genetics, 9*(9), e1003851.
840 https://doi.org/10.1371/journal.pgen.1003851
841 Howard, J. M., & Sanford, J. R. (2015). The RNAissance family: SR proteins as multifaceted
842 regulators of gene expression: *Wiley Interdisciplinary Reviews: RNA*, *6*(1), 93–110.
843 https://doi.org/10.1002/wrna.1260
844 Huang, Y., Yario, T. A., & Steitz, J. A. (2004). A molecular link between SR protein
845 dephosphorylation and mRNA export. *Proceedings of the National Academy of*
846 *Sciences*, *101*(26), 9666–9670. https://doi.org/10.1073/pnas.0403533101
847 Jourdain, A. A., Begg, B. E., Mick, E., Shah, H., Calvo, S. E., Skinner, O. S., Sharma, R., Blue,
848 S. M., Yeo, G. W., Burge, C. B., & Mootha, V. K. (2021). Loss of LUC7L2 and U1 snRNP

849 subunits shifts energy metabolism from glycolysis to OXPHOS. *Molecular Cell*, *81*(9),
850 1905-1919.e12. https://doi.org/10.1016/j.molcel.2021.02.033
851 Jumaa, H., Wei, G., & Nielsen, P. J. (1999). Blastocyst formation is blocked in mouse embryos
852 lacking the splicing factor SRp20. *Current Biology*, *9*(16), 899–902.
853 https://doi.org/10.1016/S0960-9822(99)80394-7
854 Klinghoffer, R. A., Hamilton, T. G., Hoch, R., & Soriano, P. (2002). An Allelic Series at the
855 PDGFaR Locus Indicates Unequal Contributions of Distinct Signaling Pathways During
856 Development. *Developmental Cell*, *2*(1), 103–113. https://doi.org/10.1016/s1534-
857 5807(01)00103-4
858 Krainer, R., Mayeda, A., & Kozak, D. (1991). Functional Expression of Cloned Human Splicing
859 Factor SF2: Homology to RNA-Binding Proteins, Ul 70K, and Drosophila Splicing
860 Regulators. *Cell*, *66*(2), 383–394. https://doi.org/10.1016/0092-8674(91)90627-b
861 Kuleshov, M. V., Jones, M. R., Rouillard, A. D., Fernandez, N. F., Duan, Q., Wang, Z., Koplev,
862 S., Jenkins, S. L., Jagodnik, K. M., Lachmann, A., McDermott, M. G., Monteiro, C. D.,
863 Gundersen, G. W., & Ma'ayan, A. (2016). Enrichr: A comprehensive gene set
864 enrichment analysis web server 2016 update. *Nucleic Acids Research*, *44*(W1), W90–
865 W97. https://doi.org/10.1093/nar/gkw377
866 Lee, S., Sears, M. J., Zhang, Z., Li, H., Salhab, I., Krebs, P., Xing, Y., Nah, H.-D., Williams, T., &
867 Carstens, R. P. (2020). Cleft lip and cleft palate in *Esrp1* knockout mice is associated
868 with alterations in epithelial-mesenchymal crosstalk. *Development*, *147*(21), dev187369.
869 https://doi.org/10.1242/dev.187369
870 Li, D., & Roberts, R. (2001). WD-repeat proteins: Structure characteristics, biological function,
871 and their involvement in human diseases. *Cellular and Molecular Life Sciences*, *58*(14),
872 2085-2097. https://doi.org/10.1007/pl00000838

Liao, X., Hu, K., Salhi, A., Zou, Y., Wang, J., & Gao, X. (2022). msRepDB: A comprehensive repetitive sequence database of over 80 000 species. *Nucleic Acids Research*, *50*(D1), D236–D245. https://doi.org/10.1093/nar/gkab1089

Licatalosi, D. D., & Darnell, R. B. (2010). RNA processing and its regulation: Global insights into biological networks. *Nature Reviews Genetics*, *11*(1), 75–87. https://doi.org/10.1038/nrg2673

Liu, K., Jian, Y., Sun, X., Yang, C., Gao, Z., Zhang, Z., Liu, X., Li, Y., Xu, J., Jing, Y., Mitani, S., He, S., & Yang, C. (2016). Negative regulation of phosphatidylinositol 3-phosphate levels in early-to-late endosome conversion. *Journal of Cell Biology, 212*(2), 181-198. https://doi.org/10.1083/jcb.201506081.

Long, Y., Sou, W. H., Yung, K. W. Y., Liu, H., Wan, S. W. C., Li, Q., Zeng, C., Law, C. O. K., Chan, G. H. C., Lau, T. C. K., & Ngo, J. C. K. (2019). Distinct mechanisms govern the phosphorylation of different SR protein splicing factors. *Journal of Biological Chemistry*, *294*(4), 1312–1327. https://doi.org/10.1074/jbc.RA118.003392

Love, M. I., Huber, W., & Anders, S. (2014). Moderated estimation of fold change and dispersion for RNA-seq data with DESeq2. *Genome Biology*, *15*(12), 550. https://doi.org/10.1186/s13059-014-0550-8

Mai, C. T., Isenburg, J. L., Canfield, M. A., Meyer, R. E., Correa, A., Alverson, C. J., Lupo, P. J., Riehle-Colarusso, T., Cho, S. J., Aggarwal, D., Kirby, R. S., & National Birth Defects Prevention Network. (2019). National population-based estimates for major birth defects, 2010–2014. *Birth Defects Research*, *111*(18), 1420–1435. https://doi.org/10.1002/bdr2.1589

Manning, B. D., & Cantley, L. C. (2007). AKT/PKB Signaling: Navigating Downstream. *Cell*, *129*(7), 1261–1274. https://doi.org/10.1016/j.cell.2007.06.009

Martin, M. (2011). Cutadapt removes adapter sequences from high-throughput sequencing reads. *EMBnet.Journal*, *17*(1), 10. https://doi.org/10.14806/ej.17.1.200

Miura, Y., Hongu, T., Yamauchi, Y., Funakoshi, Y., Katagiri, N., Ohbayashi, N., & Kanaho, Y. (2016). ACAP3 regulates neurite outgrowth through its GAP activity specific to Arf6 in mouse hippocampal neurons. *Biochemical Journal*, *473*(17), 2591-2602. https://doi.org/10.1042/BCJ20160183

Moss, N. D., Wells, K. L., Theis, A., Kim, Y.-K., Spigelman, A. F., Liu, X., MacDonald, P. E., & Sussel, L. (2023). Modulation of insulin secretion by RBFOX2-mediated alternative splicing. *Nature Communications*, *14*(1), 7732. https://doi.org/10.1038/s41467-023-43605-4

Pan, Q., Shai, O., Lee, L. J., Frey, B. J., & Blencowe, B. J. (2008). Deep surveying of alternative splicing complexity in the human transcriptome by high-throughput sequencing. *Nature Genetics*, *40*(12), 1413–1415. https://doi.org/10.1038/ng.259

Park, J. W., Jung, S., Rouchka, E. C., Tseng, Y-T., & Xing, Y. (2016). rMAPS: RNA map analysis and plotting server for alternative exon regulation. *Nucleic Acids Research* *44*(W1), 333-338. https://doi.org/10.1093/nar/gkw410

Patro, R., Duggal, G., Love, M. I., Irizarry, R. A., & Kingsford, C. (2017). Salmon provides fast and bias-aware quantification of transcript expression. *Nature Methods*, *14*(4), 417–419. https://doi.org/10.1038/nmeth.4197

Ramírez, F., Ryan, D. P., Grüning, B., Bhardwaj, V., Kilpert, F., Richter, A. S., Heyne, S., Dündar, F., & Manke, T. (2016). deepTools2: A next generation web server for deep-sequencing data analysis. *Nucleic Acids Research*, *44*(W1), W160–W165. https://doi.org/10.1093/nar/gkw257

Rapiteanu, R., Davis, L. J., Williamson, J. C., Timms, R. T., Paul Luzio, J., & Lehner, P. J. (2016). A Genetic Screen Identifies a Critical Role for the WDR81-WDR91 Complex in the Trafficking and Degradation of Tetherin. *Traffic*, *17*(8), 940–958. https://doi.org/10.1111/tra.12409

Rattanasopha, S., Tongkobpetch, S., Srichomthong, C., Siriwan, P., Suphapeetiporn, K., & Shotelersuk, V. (2012). PDGFRa mutations in humans with isolated cleft palate. *European Journal of Human Genetics*, *20*(10), 1058–1062. https://doi.org/10.1038/ejhg.2012.55

Riemondy, K. A., Sheridan, R. M., Gillen, A., Yu, Y., Bennett, C. G., & Hesselberth, J. R. (2017). valr: Reproducible genome interval analysis in R. *F1000Research*, *6*, 1025. https://doi.org/10.12688/f1000research.11997.1

Robinson, J. T., Thorvaldsdóttir, H., Winckler, W., Guttman, M., Lander, E. S., Getz, G., & Mesirov, J. P. (2011). Integrative genomics viewer. *Nature Biotechnology*, *29*(1), 24–26. https://doi.org/10.1038/nbt.1754

Rogers, M. A., Campaña, M. B., Long, R., & Fantauzzo, K. A. (2022). PDGFR dimer-specific activation, trafficking and downstream signaling dynamics. *Journal of Cell Science*, *135*(17), jcs259686. https://doi.org/10.1242/jcs.259686

Schmok, J. C., Jain, M., Street, L. A., Tankka, A. T., Schafer, D., Her, H.-L., Elmsaouri, S., Gosztyla, M. L., Boyle, E. A., Jagannatha, P., Luo, E.-C., Kwon, E. J., Jovanovic, M., & Yeo, G. W. (2024). Large-scale evaluation of the ability of RNA-binding proteins to activate exon inclusion. *Nature Biotechnology*. https://doi.org/10.1038/s41587-023-02014-0

Scotti, M. M., & Swanson, M. S. (2016). RNA mis-splicing in disease. *Nature Reviews Genetics*, *17*(1), 19–32. https://doi.org/10.1038/nrg.2015.3

Shen, H., & Green, M. R. (2006). RS domains contact splicing signals and promote splicing by a common mechanism in yeast through humans. *Genes & Development*, *20*(13), 1755–1765. https://doi.org/10.1101/gad.1422106

Shen, S., Park, J. W., Lu, Z., Lin, L., Henry, M. D., Wu, Y. N., Zhou, Q., & Xing, Y. (2014). rMATS: Robust and flexible detection of differential alternative splicing from replicate

949 RNA-Seq data. *Proceedings of the National Academy of Sciences*, *111*(51), E5593–
950 E5601. https://doi.org/10.1073/pnas.1419161111
951 Shin, C., Feng, Y., & Manley, J. L. (2004). Dephosphorylated SRp38 acts as a splicing
952 repressor in response to heat shock. *Nature*, *427*(6974), 553–558.
953 https://doi.org/10.1038/nature02288
954 Simpson, J. E., Muir, M. T., Lee, M., Naughton, C., Gilbert, N., Pollard, S. M., & Gammoh, N.
955 (2024). Autophagy supports PDGFRA-dependent brain tumor development by
956 enhancing oncogenic signaling. *Developmental Cell*, S1534580723006214.
957 https://doi.org/10.1016/j.devcel.2023.11.023
958 Soneson, C., Love, M. I., & Robinson, M. D. (2016). Differential analyses for RNA-seq:
959 Transcript-level estimates improve gene-level inferences [version 2; referees: 2
960 approved]. *F1000Research*, *4*, 1521. https://doi.org/10.12688/F1000RESEARCH.7563.2
961 Soriano, P. (1997). The PDGFα receptor is required for neural crest cell development and for
962 normal patterning of the somites. *Development*, *124*(14), 2691–2700.
963 https://doi.org/10.1242/dev.124.14.2691
964 Tallquist, M. D., & Soriano, P. (2003). Cell autonomous requirement for PDGFRα in populations
965 of cranial and cardiac neural crest cells. *Development*, *130*(3), 507–518.
966 https://doi.org/10.1242/dev.00241
967 Uyar, B., Yusuf, D., Wurmus, R., Rajewsky, N., Ohler, U., & Akalin, A. (2017). RCAS: An RNA
968 centric annotation system for transcriptome-wide regions of interest. *Nucleic Acids*
969 *Research*, *45*(10), e91–e91. https://doi.org/10.1093/nar/gkx120
970 Van Nostrand, E. L., Nguyen, T. B., Gelboin-Burkhart, C., Wang, R., Blue, S. M., Pratt, G. A.,
971 Louie, A. L., & Yeo, G. W. (2017). Robust, Cost-Effective Profiling of RNA Binding
972 Protein Targets with Single-end Enhanced Crosslinking and Immunoprecipitation

(seCLIP). In Y. Shi (Ed.), *mRNA Processing* (Vol. 1648, pp. 177–200). Springer New York. https://doi.org/10.1007/978-1-4939-7204-3_14

Van Nostrand, E. L., Pratt, G. A., Shishkin, A. A., Gelboin-Burkhart, C., Fang, M. Y., Sundararaman, B., Blue, S. M., Nguyen, T. B., Surka, C., Elkins, K., Stanton, R., Rigo, F., Guttman, M., & Yeo, G. W. (2016). Robust transcriptome-wide discovery of RNA-binding protein binding sites with enhanced CLIP (eCLIP). *Nature Methods*, *13*(6), 508–514. https://doi.org/10.1038/nmeth.3810

Vasudevan, H. N., Mazot, P., He, F., & Soriano, P. (2015). Receptor tyrosine kinases modulate distinct transcriptional programs by differential usage of intracellular pathways. *eLife*, *4*, e07186. https://doi.org/10.7554/eLife.07186

Wallroth, A., & Haucke, V. (2018). Phosphoinositide conversion in endocytosis and the endolysosomal system. *Journal of Biological Chemistry*, *293*(5), 1526–1535. https://doi.org/10.1074/jbc.R117.000629

Wang, E. T., Sandberg, R., Luo, S., Khrebtukova, I., Zhang, L., Mayr, C., Kingsmore, S. F., Schroth, G. P., & Burge, C. B. (2008). Alternative isoform regulation in human tissue transcriptomes. *Nature*, *456*(7221), 470–476. https://doi.org/10.1038/nature07509

Xiao, S. H., & Manley, J. (1997). Phosphorylation of the ASF/SF2 RS domain affects both protein-protein and protein-RNA interactions and is necessary for splicing. *Genes & Development*, *11*(3), 334-344. https://doi.org/10.1101/gad.11.3.334

Yee, B. A., Pratt, G. A., Graveley, B. R., Van Nostrand, E. L., & Yeo, G. W. (2019). RBP-Maps enables robust generation of splicing regulatory maps. *RNA*, *25*(2), 193-204. https://doi.org/10.1261/rna.069237.118

Yoo, J. H., Brady, S. W., Acosta-Alvarez, L., Rogers, A., Peng, J., Sorensen, L. K., Wolff, R. K., Mleynek, T., Shin, D., Rich, C. P., Kircher, D. A., Bild, A., Odelberg, S. J., Li, D. Y., Holmen, S. L., & Grossmann, A. H. (2019). The small GTPase ARG5 activates PI3K in

998 melanoma to induce a prometastatic state. *Cancer Research, 79*(11), 2892-2908.
999 https://doi.org/10.1158/0008-5472.CAN-18-3026
1000 Zahler, A. M., Neugebauer, K. M., Lane, W. S., & Roth, M. B. (1993). Distinct Functions of SR
1001 Proteins in Alternative pre-mRNA Splicing. *Science*, *260*(5105), 219–222.
1002 https://doi.org/10.1126/science.8385799
1003 Zerial, M., & McBride, H. (2001). Rab proteins as membrane organizers. *Nature Reviews*
1004 *Molecular Cell Biology*, *2*(2), 107–117. https://doi.org/10.1038/35052055
1005 Zhou, Z., & Fu, X.-D. (2013). Regulation of splicing by SR proteins and SR protein-specific
1006 kinases. *Chromosoma*, *122*(3), 191–207. https://doi.org/10.1007/s00412-013-0407-z
1007 Zhou, Z., Qiu, J., Liu, W., Zhou, Y., Plocinik, R. M., Li, H., Hu, Q., Ghosh, G., Adams, J. A.,
1008 Rosenfeld, M. G., & Fu, X.-D. (2012). The Akt-SRPK-SR Axis Constitutes a Major
1009 Pathway in Transducing EGF Signaling to Regulate Alternative Splicing in the Nucleus.
1010 *Molecular Cell*, *47*(3), 422–433. https://doi.org/10.1016/j.molcel.2012.05.014
1011

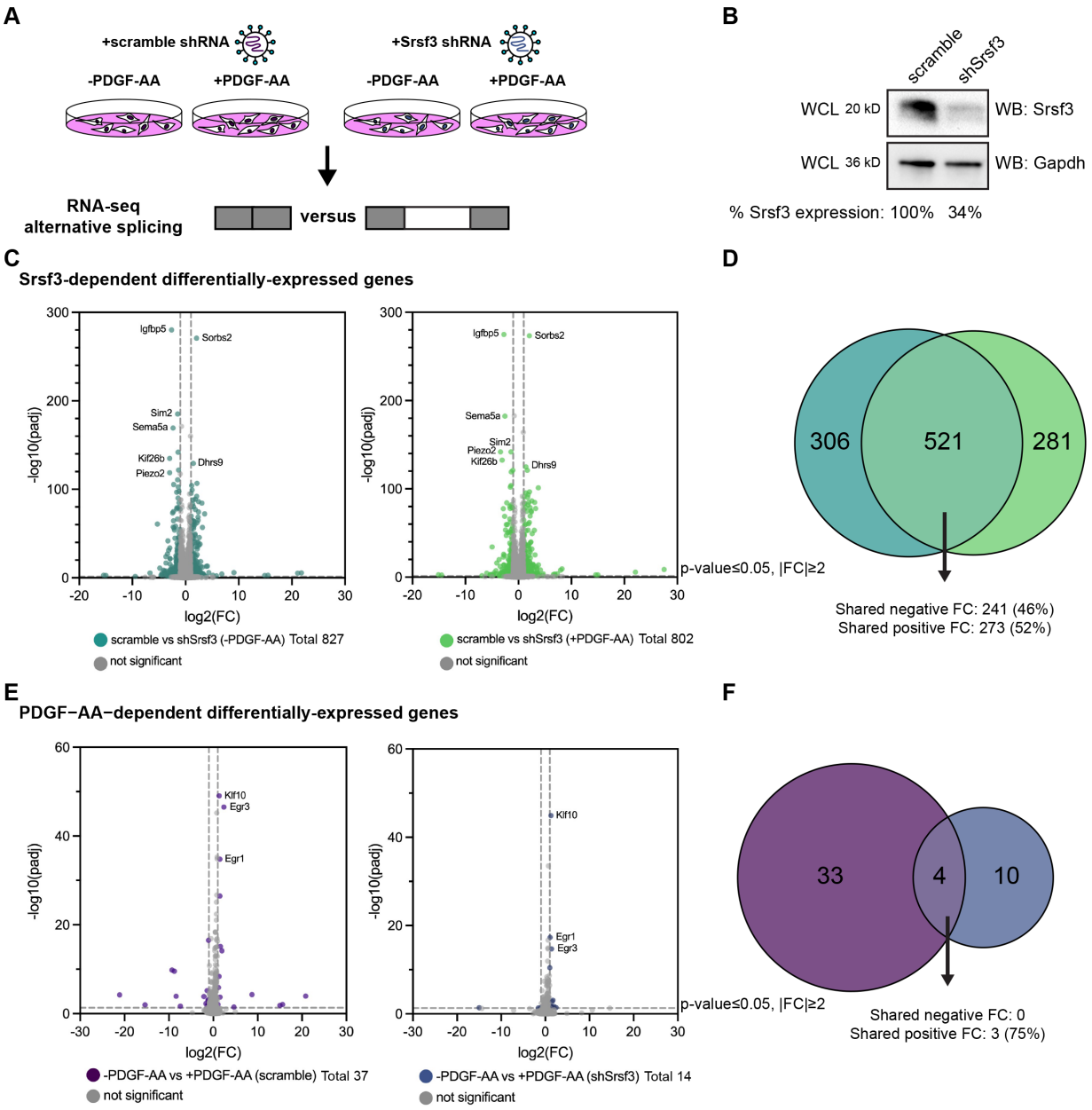

Figure 1: PDGFRα signaling for one hour minimally affects gene expression. (A) Schematic of RNA-seq experimental design. iMEPM cells were transduced to stably express a scramble shRNA (scramble) or shRNA targeting the 3' UTR of *Srsf3* (shSrsf3). iMEPM cells expressing either scramble or shSrsf3 were left unstimulated or stimulated with 10 ng/mL PDGF-AA for 1 hour and RNA was isolated for RNA-seq analysis. **(B)** Western blot (WB) analysis of whole-cell lysates (WCL) from scramble and shSrsf3 cell lines with anti-Srsf3 and

1019 anti-Gapdh antibodies. The percentage of Srsf3 expression normalized to Gapdh expression is
1020 indicated below. **(C)** Volcano plots depicting differentially-expressed genes in scramble versus
1021 shSrsf3 cell lines in the absence (left) or presence (right) of PDGF-AA stimulation. Log_2(fold
1022 change) (FC) values represent log_2(shSrsf3 normalized counts/scramble normalized counts).
1023 Significant changes in gene-level expression are reported for genes with adjusted *P* (padj) <
1024 0.05 and fold change $|FC| \geq 2$. **(D)** Venn diagram of significant genes from C. **(E)** Volcano plots
1025 depicting differentially-expressed genes in the absence versus presence of PDGF-AA ligand in
1026 scramble (left) or shSrsf3 (right) cell lines. Log_2(FC) values represent log_2(+PDGF-AA
1027 normalized counts/-PDGF-AA normalized counts). **(F)** Venn diagram of significant genes from
1028 E.
1029

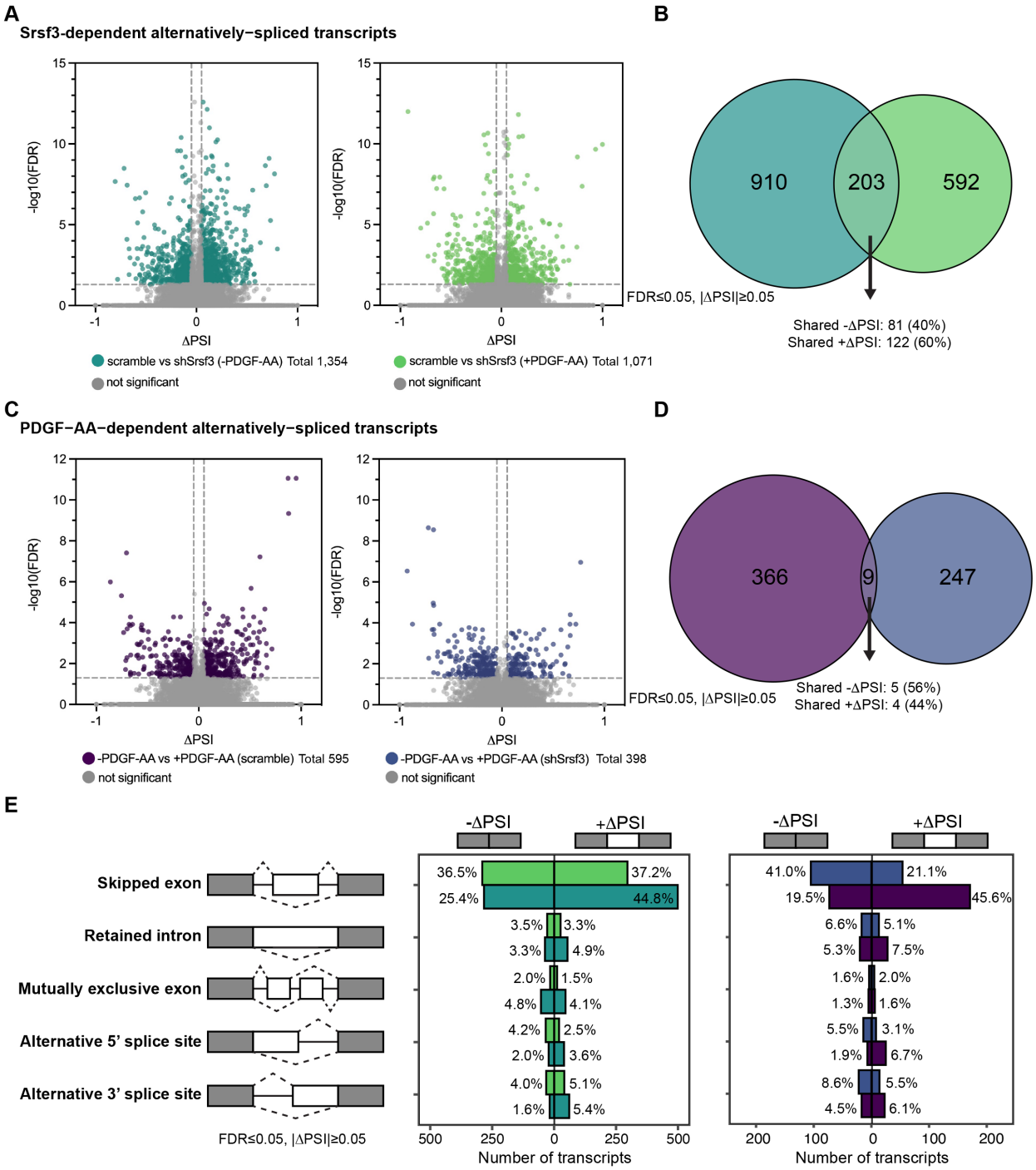

Figure 2: PDGFRα signaling for one hour has a more pronounced effect on alternative RNA splicing. (A) Volcano plots depicting alternatively-spliced transcripts in scramble versus shSrsf3 cell lines in the absence (left) or presence (right) of PDGF-AA stimulation. Difference in percent spliced in (ΔPSI) values represent scramble PSI – shSrsf3 PSI. Significant changes in

1035 alternative RNA splicing are reported for events with a false discovery rate (FDR) $\leq$ 0.05 and a
1036 difference in percent spliced in (|ΔPSI|) $\geq$ 0.05. **(B)** Venn diagram of significant transcripts from
1037 A, filtered to include events detected in at least 10 reads in either condition. **(C)** Volcano plots
1038 depicting alternatively-spliced transcripts in the absence versus presence of PDGF-AA ligand in
1039 scramble (left) or shSrsf3 (right) cell lines. Difference in percent spliced in (ΔPSI) values
1040 represent -PDGF-AA PSI – +PDGF-AA PSI. **(D)** Venn diagram of significant transcripts from C,
1041 filtered to include events detected in at least 10 reads in either condition. **(E)** Bar graphs
1042 depicting alternative RNA splicing events in scramble versus shSrsf3 cell lines in the absence or
1043 presence of PDGF-AA stimulation (left) or in the absence versus presence of PDGF-AA ligand
1044 in scramble or shSrsf3 cell lines (right).
1045

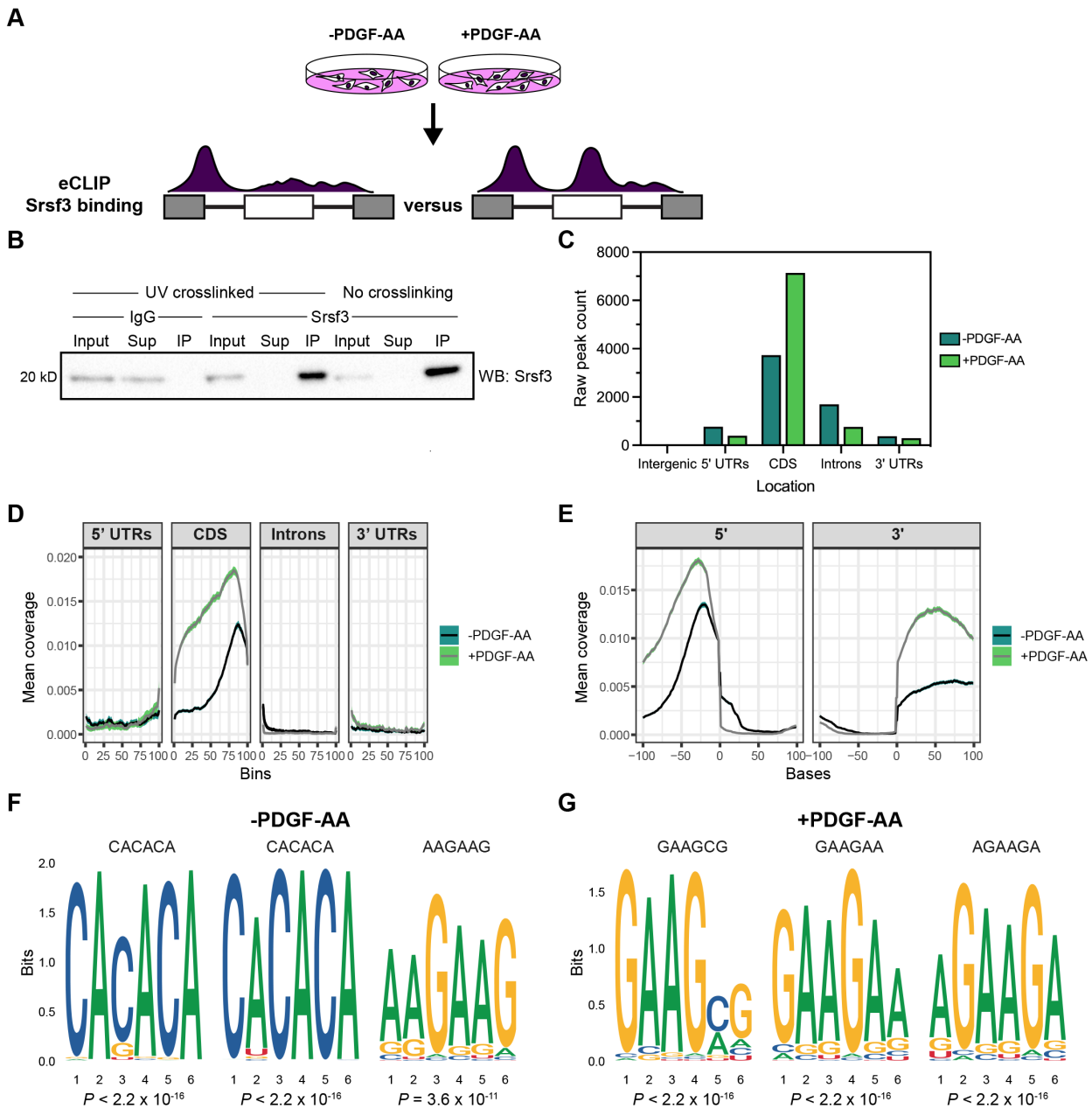

Figure 3: Srsf3 exhibits differential transcript binding upon PDGFRα signaling. (A) Schematic of eCLIP experimental design. iMEPM cells were left unstimulated or stimulated with 10 ng/mL PDGF-AA for 1 hour and processed for eCLIP analysis. **(B)** Immunoprecipitation (IP) of Srsf3 from cells that were UV-crosslinked or not UV-crosslinked with IgG or an anti-Srsf3 antibody followed by western blotting (WB) of input, supernatant (Sup), and IP samples with an anti-Srsf3 antibody. **(C)** Mapping of eCLIP peaks to various transcript locations in the absence

1053 or presence of PDGF-AA stimulation. 5’ UTR, 5’ untranslated region; CDS, coding sequence; 3’
1054 UTR, 3’ untranslated region. **(D,E)** Mean coverage of eCLIP peaks across various transcript
1055 locations (D) and surrounding the 5’ and 3’ splice sites (E) in the absence or presence of PDGF-
1056 AA stimulation. **(F,G)** Top three motifs enriched in eCLIP peaks in the absence (F) or presence
1057 (G) of PDGF-AA stimulation with associated *P* values.
1058

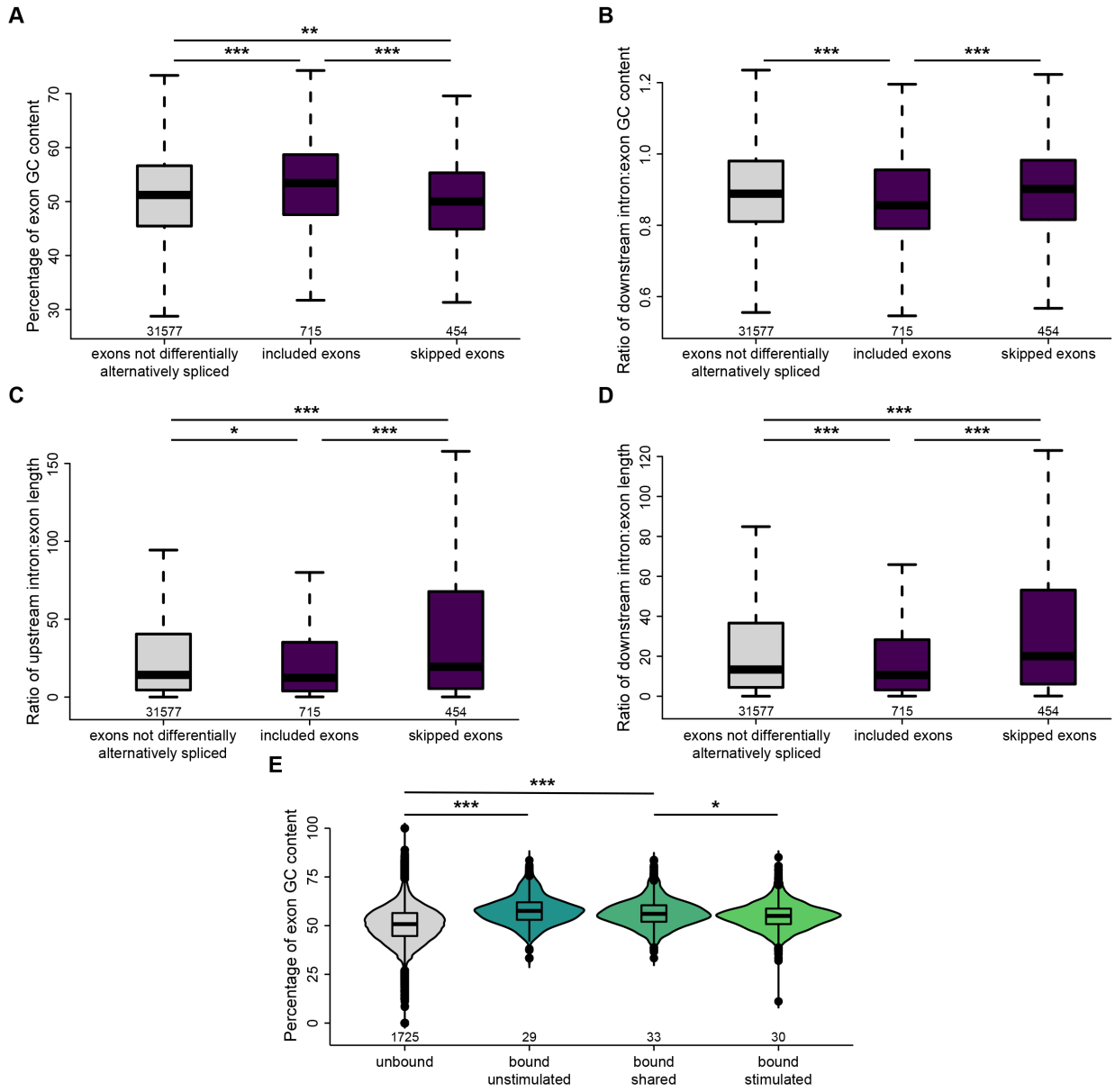

Figure 4: Srsf3 and PDGFRα signaling are associated with differential GC content and length of alternatively-spliced exons. (A) Box and whisker plot depicting the percentage of exon GC content in exons that are not differentially alternatively spliced, and exons that are included or skipped when Srsf3 is present from the rMATS analysis. **(B)** Box and whisker plot depicting the ratio of downstream intron to exon GC content in exons that are not differentially alternatively spliced, and exons that are included or skipped when Srsf3 is present from the rMATS analysis. **(C,D)** Box and whisker plots depicting the ratio of upstream intron to exon

1067 length (C) and downstream intron to exon length (D) in exons that are not differentially
1068 alternatively spliced, and exons that are included or skipped when Srsf3 is present from the
1069 rMATS analysis. **(E)** Violin and box and whisker (inset) plots depicting the percentage of exon
1070 GC content in exons that are not bound by Srsf3, and exons that are bound in the absence
1071 and/or presence of PDGF-AA stimulation from the eCLIP analysis. *, $P < 0.05$; **, $P < 0.01$; ***,
1072 $P < 0.001$.
1073

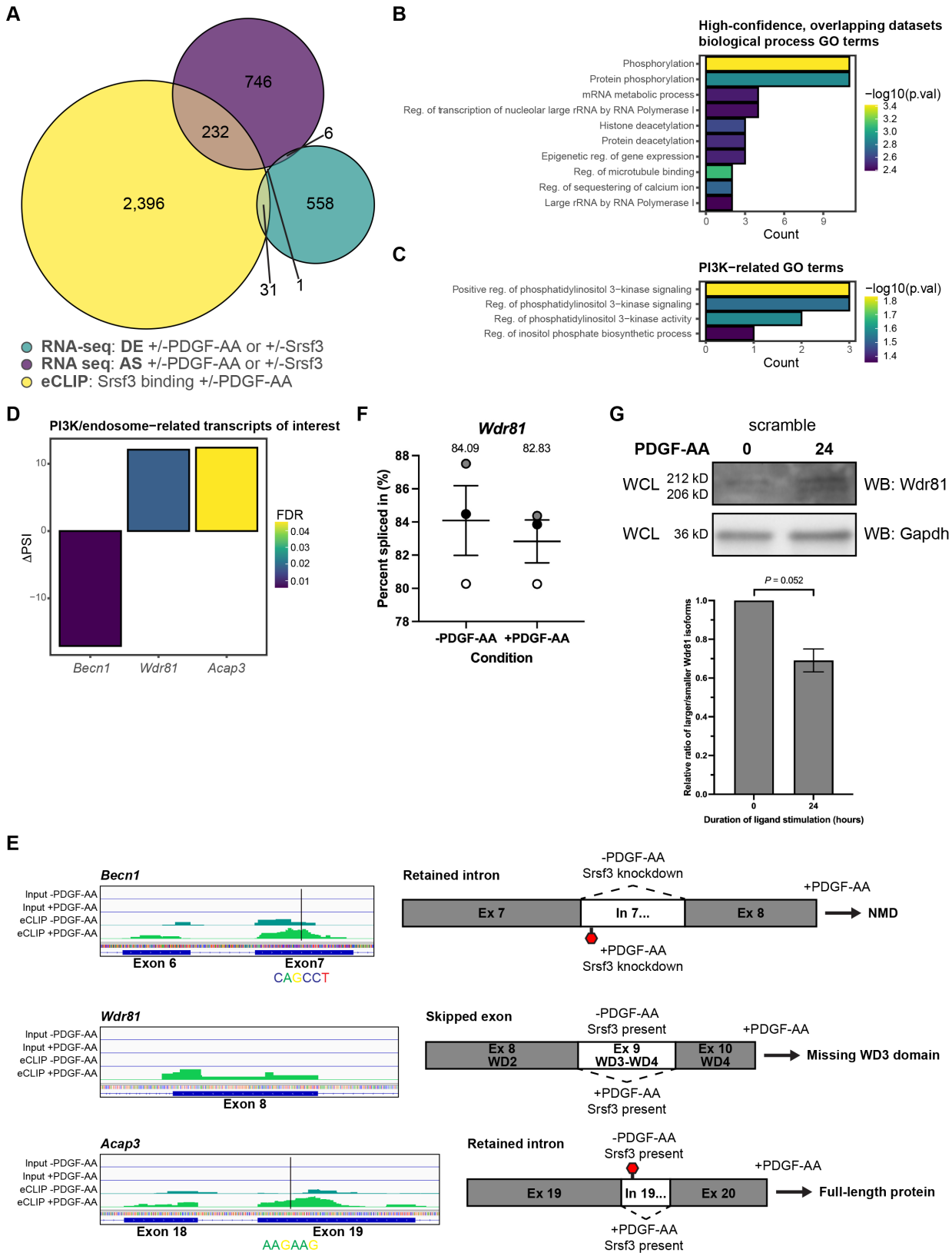
A
746
232
6
2,396
558
31
1
RNA-seq: DE +/-PDGF-AA or +/-Srsf3
RNA seq: AS +/-PDGF-AA or +/-Srsf3
eCLIP: Srsf3 binding +/-PDGF-AA
B
High-confidence, overlapping datasets biological process GO terms
Phosphorylation
Protein phosphorylation
mRNA metabolic process
Reg. of transcription of nucleolar large rRNA by RNA Polymerase I
Histone deacetylation
Protein deacetylation
Epigenetic reg. of gene expression
Reg. of microtubule binding
Reg. of sequestering of calcium ion
Large rRNA by RNA Polymerase I
Count
−log10(p.val)
C
PI3K−related GO terms
Positive reg. of phosphatidylinositol 3−kinase signaling
Reg. of phosphatidylinositol 3−kinase signaling
Reg. of phosphatidylinositol 3−kinase activity
Reg. of inositol phosphate biosynthetic process
Count
−log10(p.val)
D
PI3K/endosome−related transcripts of interest
ΔPSI
FDR
Becn1
Wdr81
Acap3
F
Wdr81
84.09
82.83
Percent spliced in (%)
-PDGF-AA
+PDGF-AA
Condition
G
scramble
PDGF-AA
0
24
WCL
212 kD
206 kD
WB: Wdr81
WCL
36 kD
WB: Gapdh
P = 0.052
Relative ratio of larger/smaller Wdr81 isoforms
Duration of ligand stimulation (hours)
E
Becn1
Input -PDGF-AA
Input +PDGF-AA
eCLIP -PDGF-AA
eCLIP +PDGF-AA
Exon 6
Exon7
CAGCCT
Retained intron
-PDGF-AA
Srsf3 knockdown
+PDGF-AA
Ex 7
In 7...
Ex 8
NMD
+PDGF-AA
Srsf3 knockdown
Wdr81
Exon 8
Skipped exon
-PDGF-AA
Srsf3 present
+PDGF-AA
Ex 8
WD2
Ex 9
WD3-WD4
Ex 10
WD4
Missing WD3 domain
+PDGF-AA
Srsf3 present
Acap3
Exon 18
Exon 19
AAGAAG
Retained intron
-PDGF-AA
Srsf3 present
+PDGF-AA
Ex 19
In 19...
Ex 20
Full-length protein
+PDGF-AA
Srsf3 present

1074

1075 **Figure 5: Transcripts bound by Srsf3 that undergo alternative splicing upon PDGFRα**
1076 **signaling encode regulators of PI3K signaling. (A)** Venn diagram of genes with differential
1077 expression (DE) or transcripts subject to alternative RNA splicing (AS) across the four treatment
1078 comparisons that overlap with transcripts with Srsf3 eCLIP peaks in the absence or presence of
1079 PDGF-AA stimulation. **(B,C)** Top ten (B) and PI3K-related (C) biological process gene ontology
1080 (GO) terms for transcripts from the high-confidence, overlapping datasets. p.val, *P*. **(D)**
1081 Difference in percent spliced in (ΔPSI) values for PI3K/endosome-related transcripts of interest.
1082 ΔPSI values represent -PDGF-AA PSI – +PDGF-AA PSI. FDR, false detection rate. **(E)** Peak
1083 visualization for input and eCLIP samples in the absence or presence of PDGF-AA stimulation
1084 from Integrative Genomics Viewer (left) with location of motifs from Figure S6 indicated below
1085 for PI3K/endosome-related transcripts of interest. Predicted alternative splicing outcomes for
1086 PI3K/endosome-related transcripts of interest (right). **(F)** Scatter dot plot depicting the percent
1087 spliced in as assessed by qPCR analysis of *Wdr81* exon 9 in the scramble cell line following 1 h
1088 of PDGF-AA stimulation quantified from n = 3 biological replicates. Data are mean ± s.e.m.
1089 Shaded circles correspond to independent experiments. **(G)** Western blot (WB) analysis of
1090 whole-cell lysates (WCL) from the scramble cell line following 24 h of PDGF-AA stimulation with
1091 anti-Wdr81 and anti-Gapdh antibodies. Bar graph depicting relative ratios of larger/smaller
1092 Wdr81 isoforms quantified from n = 3 biological replicates as above. Data are mean ± s.e.m.
1093

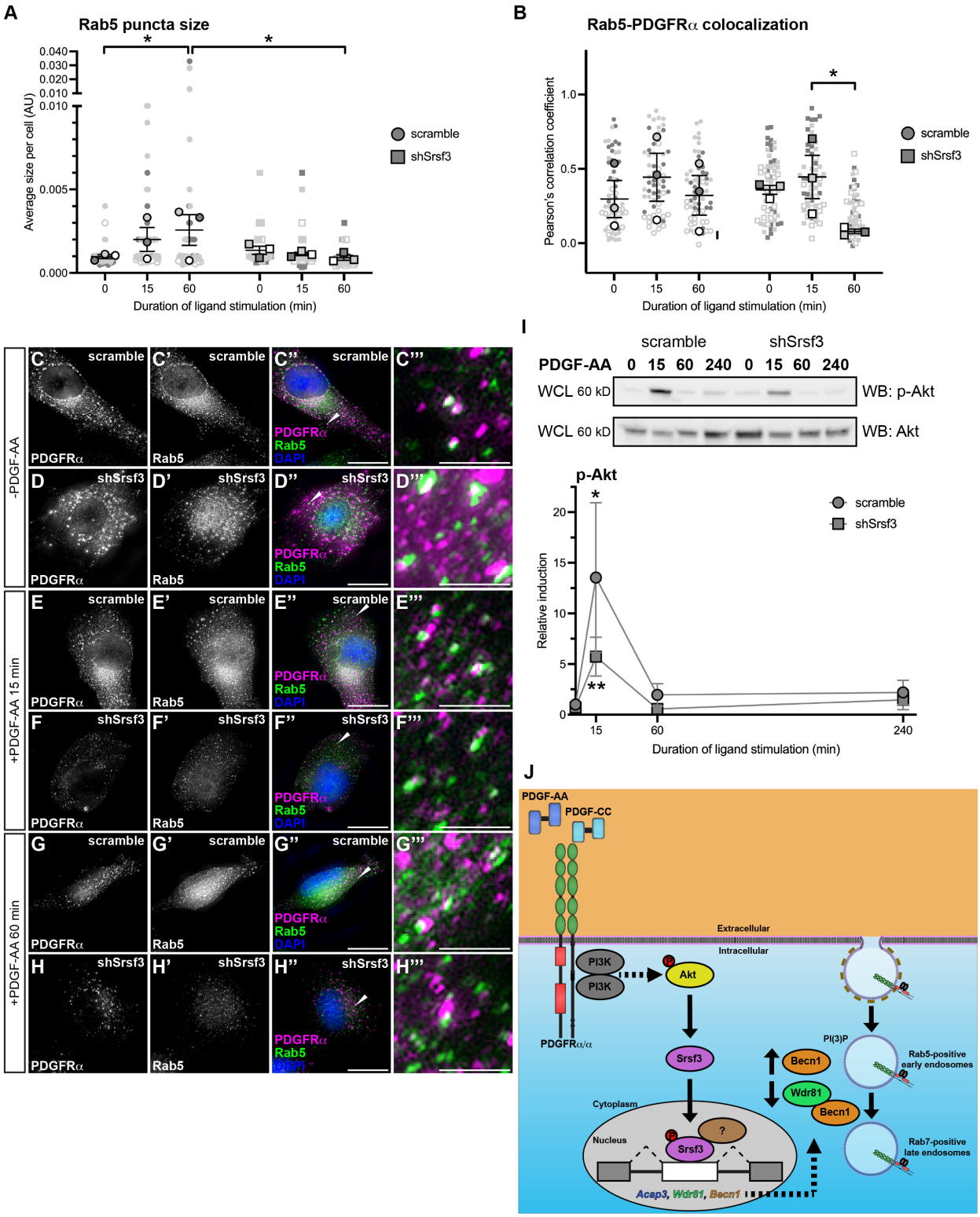

Figure 6: Srsf3 regulates early endosome size and phosphorylation of Akt downstream of PDGFRα signaling. (A,B) Scatter dot plots depicting average size of Rab5 puncta per cell (A)

1097 and Pearson's correlation coefficient of signals from anti-Rab5 and anti-PDGFRα antibodies (B)
1098 in scramble and shSrsf3 cell lines in the absence or presence (15-60 min) of PDGF-AA
1099 stimulation. Data are mean ± s.e.m. *, $P < 0.05$. Shaded shapes correspond to independent
1100 experiments. Summary statistics from biological replicates consisting of independent
1101 experiments (large shapes) are superimposed on top of data from all cells; $n = 20$ technical
1102 replicates across each of three biological replicates. **(C-H''')** PDGFRα antibody signal (white or
1103 magenta) and Rab5 antibody signal (white or green) as assessed by immunofluorescence
1104 analysis of scramble and shSrsf3 cells in the absence or presence (15-60 min) of PDGF-AA
1105 stimulation. Nuclei were stained with DAPI (blue). White arrows denote regions of colocalization,
1106 which are expanded in C'''-H'''. Scale bars: 20 μm (C-H''), 3 μm (C'''-H'''). **(I)** Western blot (WB)
1107 analysis of whole-cell lysates (WCL) from scramble (left) and shSrsf3 (right) cell lines following a
1108 time course of PDGF-AA stimulation from 15 min to 4 h, with anti-phospho-(p)-Akt and anti-Akt
1109 antibodies. Line graph depicting quantification of band intensities from $n = 3$ biological replicates
1110 as above. Data are mean ± s.e.m. *, $P < 0.05$; **, $P < 0.01$. **(J)** Model of experimental results in
1111 which PI3K/Akt-mediated PDGFRα signaling results in the nuclear translocation of Srsf3 and
1112 the subsequent AS of transcripts to decrease levels of proteins that promote PDGFRα
1113 trafficking out of early endosomes.